

Formation of highly oxygenated organic molecules from the oxidation of limonene by OH radical: significant contribution of H-abstraction pathway

Hao Luo^{1,2}, Luc Vereecken³, Hongru Shen^{1,2}, Sungah Kang³, Iida Pullinen^{3a}, Mattias Hallquist⁴, Hendrik Fuchs^{3,5}, Andreas Wahner³, Astrid Kiendler-Scharr^{3†}, Thomas F Mentel^{3*}, Defeng Zhao^{1,2,6,7,8*}

¹Department of Atmospheric and Oceanic Sciences & Institute of Atmospheric Sciences, Fudan University, Shanghai, 200438, China

²National Observations and Research Station for Wetland Ecosystems of the Yangtze Estuary, Fudan University, Shanghai, 200438, China

³Institute of Energy and Climate Research, IEK-8: Troposphere, Forschungszentrum Jülich, Jülich, 52425, Germany

⁴Department of Chemistry and Molecular biology, University of Gothenburg, Göteborg, 41258, Sweden

⁵[Fachgruppe Physik, Universität zu Köln, Cologne, 50932, Germany](#)

⁶Shanghai Frontiers Science Center of Atmosphere-Ocean Interaction, Fudan University, Shanghai 200438, China

⁷Institute of Eco-Chongming (IEC), 20 Cuinia Rd., Chongming, Shanghai, 202162, China

⁸CMA-FDU Joint Laboratory of Marine Meteorology, Fudan University, Shanghai 200438, China

^aNow at: Department of Applied Physics, University of Eastern Finland, Kuopio, 70210, Finland

[†][deceased on 6 February 2023](#)

Correspondence to: Defeng Zhao (dfzhao@fudan.edu.cn), Thomas F Mentel (t.mentel@fz-juelich.de)

Abstract. Highly oxygenated organic molecules (HOM) play a pivotal role in the formation of secondary organic aerosol (SOA). Therefore, the distribution and yields of HOM are fundamental to understand their fate and chemical evolution in the atmosphere, and it is conducive to ultimately assess the impact of SOA on air quality and climate change. In this study, gas-phase HOM formed from the reaction of limonene with OH radical in photooxidation were investigated in the SAPHIR chamber (Simulation of Atmospheric PHotochemistry In a large Reaction chamber) using a time-of-flight chemical ionization mass spectrometer with nitrate reagent ion (NO_3^- -CIMS). A large number of HOM, including monomers (C_{9-10}) and dimers (C_{17-20}), were detected and classified into various families. Both closed-shell products and open-shell peroxy radicals (RO_2), were identified under low NO (0.06 - 0.1 ppb) and high NO conditions (17 ppb). C_{10} monomers are the most abundant HOM products and account for over 80% total HOM. Closed-shell C_{10} monomers were formed from two peroxy radical families, $\text{C}_{10}\text{H}_{15}\text{O}_x\cdot$ ($x=6-15$) and $\text{C}_{10}\text{H}_{17}\text{O}_x\cdot$ ($x=6-15$), and their respective termination reactions with NO, RO_2 , and HO_2 . While $\text{C}_{10}\text{H}_{17}\text{O}_x\cdot$ is likely formed by OH addition to $\text{C}_{10}\text{H}_{16}$, the dominant initial step of limonene+OH, $\text{C}_{10}\text{H}_{15}\text{O}_x\cdot$, is likely formed via H-abstraction by OH. $\text{C}_{10}\text{H}_{15}\text{O}_x\cdot$ and related products contributed 41% and 42% of C_{10} -HOM at low and high NO, demonstrating that H-abstraction pathways play a significant role in HOM formation in the reaction of limonene+OH. Combining theoretical kinetic calculations, structure activity relationships (SARs), literature data, and the observed RO_2 intensities, we proposed tentative mechanisms of HOM formation from both pathways. We further estimated the molar yields of HOM to be $1.97_{-1.06}^{+2.52}\%$ and $0.29_{-0.16}^{+0.38}\%$ at low and high NO, respectively. Our study highlights the importance of H-abstraction by OH and provides yield and tentative pathways in the OH oxidation of limonene to simulate the HOM formation and assess their role in SOA formation.

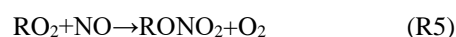
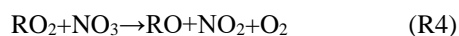
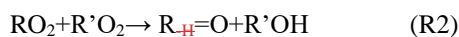
1 Introduction

Biogenic volatile organic compounds (BVOC) are important precursors of atmospheric secondary organic aerosol particles (SOA) (Griffin et al., 1999; Kanakidou et al., 2005; Hallquist et al., 2009). In the Earth's atmosphere, monoterpenes ($\text{C}_{10}\text{H}_{16}$) are abundant BVOC with the second largest emission rate of approximately 150 Tg/year (Guenther et al., 2012). Among them, limonene accounts for 20% of total monoterpene emissions, ranking as the fourth largest (Guenther et al., 2012). In addition,

as an important ingredient of essential oil and common volatile chemical product (VCP), limonene is also widely used in house cleaning and personal care products due to its pleasant fragrance and antimicrobial property. Hence, limonene can play an important role in indoor SOA formation and indoor air quality (Waring, 2016; Rossignol et al., 2013; Nazaroff and Weschler, 45 2004). Although its concentration in the atmosphere is not the most abundant among monoterpenes, limonene has a high potential to form SOA due to its high SOA yield and high reactivity provided by the presence of an endocyclic and an exocyclic double-bond (Koch et al., 2000; Chen and Hopke, 2010; Gong et al., 2018; Saathoff et al., 2009).

Limonene can undergo gas-phase reactions rapidly with atmospheric oxidants such as the hydroxyl radical (OH) and ozone (O₃) in daytime and the nitrate radical (NO₃) and O₃ in nighttime forming peroxy radicals (RO₂) (Lee et al., 2006b; Eddingsaas 50 et al., 2012; Vereecken and Peeters, 2012; Zhang et al., 2018; Yu et al., 1999; Vereecken and Peeters, 2000). In the reaction of limonene with OH, the main atmospheric daytime loss process of limonene, OH addition to one of the olefinic carbon atoms is the dominant channel, although abstraction of an allylic hydrogen atom also occurs (Rio et al., 2010; Jokinen et al., 2014). Via OH addition, the reaction forms C₁₀H₁₇O₃• as a first-generation RO₂, which under oxidative conditions further react with RO₂, HO₂, and NO forming oxidation products including limonaldehyde (C₁₀H₁₆O₂), limonaketone (C₉H₁₄O), limonic acid 55 (C₁₀H₁₆O₃), ketolimononic acid (C₉H₁₄O₄), peroxy-pinic acid or its isomer (C₁₀H₁₄O₅), nitric acid ester (C₉H₁₃NO₇), some organic acids with low molecular weight (formic acid, acetic acid, butyric acid, methacrylic), and formaldehyde (HCHO) (Pang et al., 2022; Friedman and Farmer, 2018; Romonosky et al., 2015; Jaoui et al., 2006; Lee et al., 2006a; Hakola et al., 1994). Although earlier studies have gained valuable insights into the products and mechanism of the reaction with OH, many products and their formation mechanisms are not well elucidated. For example, highly oxygenated organic molecules (HOM) 60 products and their formation mechanism remain elusive.

HOM was first discovered to be produced in forests and is defined as compounds containing six or more oxygen atoms formed in the gas phase via autoxidation (Bianchi et al., 2019; Ehn et al., 2012; Ehn et al., 2014). Among the myriad of oxygenated products, HOM was found of great importance for the mass of SOA, new particle formation and particle growth (Jokinen et al., 2015; Jokinen et al., 2014; Ehn et al., 2014; Mentel et al., 2015; Molteni et al., 2019; Kirkby et al., 2016; 65 McFiggans et al., 2019; Crouse et al., 2013; Kenseth et al., 2018; Ehn et al., 2017; Krechmer et al., 2015; Quéléver et al., 2019; Tröstl et al., 2016). Typically, HOM are generated from the autoxidation of peroxy radicals (RO₂), where a new, more oxygenated RO₂ can be formed after an intramolecular H-shift followed by O₂ addition in the resulting alkyl radical (Bianchi et al., 2019; Vereecken and Nozière, 2020; Crouse et al., 2013; Møller et al., 2019; Vereecken et al., 2007; Ehn et al., 2017; Nozière and Vereecken, 2019; Ehn et al., 2014). Bimolecular termination of the autoxidation chain occurs when an RO₂ 70 intermediate react with HO₂, RO₂, and NO to form a series of products (see below), which can be classified as organic hydroperoxide (ROOH, R1_a), alcohol (ROH, R2), and carbonyl (R=O, R2), alkoxy radicals (RO, R3-4), or organic nitrates (ON, R5). The molecular masses of termination products are M+1, M-15, M-17 and M+30, respectively, for an RO₂ with molecular mass of M (Mentel et al., 2015; Ehn et al., 2014). Meanwhile, unimolecular termination pathways generally lead to the formation of carbonyls (R=O, R6). In addition, two RO₂ can also undergo an accretion reaction to form HOM dimers (R7) 75 as the reactions shown below (Berndt et al., 2018a; Valiev et al., 2019; Zhao et al., 2018b). Note that RO₂ reaction in R2 is considered for primary and secondary RO₂. For tertiary RO₂s, carbonyls cannot be formed. In addition, the unimolecular isomerization of RO (from R1b and R3-4) could produce RO₂ in the same RO₂ family.



HOM formation in OH-initiated oxidation of monoterpenes such as α -pinene and β -pinene has been studied in the laboratory (Berndt, 2021; Xu et al., 2019; Berndt et al., 2016; Kirkby et al., 2016; Ehn et al., 2014; Shen et al., 2022), and is assumed to mainly start with the OH addition to C=C double bond. The alkyl radical adduct can rapidly add O₂ to the radical site to form a peroxy radical (Finlayson-Pitts and Pitts, 2000; Ziemann and Atkinson, 2012). A number of monomers and dimers products from several monoterpenes following the reaction with hydroxyl radical (OH) were observed, such as C₁₀H₁₄₋₁₈O₇₋₁₁ and C₁₉₋₂₀H₂₈₋₃₂O₁₀₋₁₈ (Berndt et al., 2018a; Shen et al., 2022; Xu et al., 2019). Despite the molecular similarities of HOM monomers or dimers products from different monoterpenes (Jokinen et al., 2015; Ehn et al., 2014; Ehn et al., 2012), HOM yields are quite different between different monoterpenes in a given oxidation reaction (e.g. with O₃ or OH radical) (Jokinen et al., 2015). It follows that the HOM formation mechanisms for other monoterpenes may not necessarily be applicable to limonene. Although HOM formation from limonene by ozonolysis and NO₃ has been reported (Jokinen et al., 2015; Guo et al., 2022; Mayorga et al., 2022), to the best of our knowledge, no studies have systematically reported HOM distribution in limonene+OH. In the ozonolysis of limonene, Jokinen et al. (2014) attributed some HOM (C₁₀H₁₇O_x•_(x=5,7,9) (RO₂)) to the reaction of limonene with OH produced in ozonolysis by comparing the mass spectra in the presence or absence of an OH scavenger. The composition and the formation mechanism of HOM in limonene photooxidation by OH remains unclear. Moreover, although the HOM yield of limonene+OH was determined, this yield was estimated based on the difference of the HOM yield in the ozonolysis with and without OH scavenger (HOM yields: 5.3% (limonene+O₃); 0.93% (limonene+OH)) (Jokinen et al., 2015). It is necessary to confirm the yield by its direct determination in the reaction of limonene+OH. Interestingly, in our previous study, we found that hydrogen abstraction is important for HOM formation in the reaction of α -pinene+OH (Shen et al., 2022), where intermediate alkoxy radicals oxidation steps aid autoxidation by breaking the six-membered and four-membered rings. As limonene+OH is known to have a high H-abstraction contribution of ~34% (Rio et al., 2010; Dash and Rajakumar, 2015; Braure et al., 2014), it is interesting to compare these two systems due to the similar but subtly different structures of α -pinene and limonene, with both containing a six-membered ring whereas limonene does not contain a four-membered ring.

In this study, we investigated HOM from the photooxidation of limonene with OH at low NO (0.06 - 0.1 ppb) and high NO (17 ppb) in the SAPHIR chamber at Forschungszentrum Jülich. HOM were classified into monomers and dimers, and the product distribution is reported. The yields of HOM from limonene with OH were estimated. Formation mechanism of HOM in the OH reaction is proposed based on molecular formula of HOM and quantum chemical calculation as well as structure activity relationships (SARs) of RO₂ autoxidation rates. The relative importance of OH addition to C=C double bond and hydrogen abstraction by OH is discussed. We further investigated the effects of NO_x, which changes HOM composition via altering the RO₂ fate.

115 2 Methodology

2.1 Experiment design and set-up

The experiments were conducted in the “SAPHIR” chamber (Simulation of Atmospheric PHotochemistry In a large Reaction chamber) at Forschungszentrum Jülich, Germany. The details of the chamber have been described in the previous studies (Zhao et al., 2018a; Zhao et al., 2015b; Zhao et al., 2015a; Zhao et al., 2021; Rohrer et al., 2005; Shen et al., 2021; Guo et al., 2022). In brief, SAPHIR is a 270 m³ Teflon chamber equipped with a louvre system to switch between natural sunlight for illumination and dark conditions. In this study, the experiments were conducted in sun light with the louvres opened. To avoid possible interference due to long reaction time, the subsequent discussion focuses on the early stage (15 min) of the experiment. The initial experimental conditions are shown in Table S1.

Gas and particle phase species were characterized by a comprehensive set of instruments with the details described before (Zhao et al., 2015b). A Proton Transfer Reaction Time-of-Flight Mass Spectrometer (PTR-ToF-MS, Ionicon Analytik, Austria)

was used for measuring VOC. A NO_x analyzer (ECO PHYSICS TR480) and an UV photometer O₃ analyzer (ANSYCO, model O341M) were used to measure the concentrations of NO₂, NO and O₃, respectively. A laser induced fluorescence system (LIF) was used to measure the concentrations of OH, HO₂ and RO₂ (Fuchs et al., 2012). Note that the potential artefact in HO₂ measurements from the concurrent chemical conversion of RO₂ in instrument making use of chemical conversion of HO₂ by the reaction with NO can be avoided in this study through NO used, so that no corrections of HO₂ concentration measurements are required. The detection of RO₂ radicals relies on the conversion of RO₂ to HO₂ in their reactions with NO. We applied a correction to RO₂ concentrations (Fuchs et al., 2011). We would like to note that only a few nitrated RO₂ were observed to not form HO₂ in the reaction with NO. In this study, we do not expect that there were a large contribution of nitrate RO₂ to the sum of all RO₂ as in photochemistry experiments, as there is no significant fraction of nitrate RO₂ formed. A Scanning Mobility Particle Sizer Spectrometer (SMPS, TSI, DMA3081/CPC3785) was used to obtain particle number distributions. Temperature and relative humidity were continuously measured.

Before an experiment was conducted, the chamber was flushed with high purity synthetic air (purity>99.9999% N₂ and O₂). Experiments were conducted at ~75% RH initially. In low NO condition, no NO was added and the background concentration of NO, which mainly stems from HONO photolysis produced via a photolytic process from Teflon wall, is 0.06 - 0.1 ppb (Fig. S1). OH radicals were generated from the photolysis of HONO in both low and high NO experiments and the HONO was formed from the Teflon chamber wall via a photolytic process. The details have been described by Rohrer et al. (2005). HO₂ was produced from the reaction of O₂ with RO, which can be formed in the reaction of RO₂+NO in photo-oxidation during the experiments. The concentration of limonene was 7 ppb. The reaction time after the roof opened was 8 hours. At high NO condition, 17 ppb NO was added into the chamber first and limonene was sequentially added after half an hour. The louvres were opened ~40 min after adding limonene. To estimate the impact of ozone oxidation during photooxidation, we calculated the reaction rates of VOC+OH and VOC+O₃ in the experiments of this study (Fig. S2). During the first 15 min, VOC+OH accounted for >99% limonene loss in both low and high NO condition. We would like to note that the low NO does not refer to the case where RO₂ loss is dominated by the reaction with HO₂, e.g., in remote ocean environment. At low NO the RO₂ loss was estimated to be dominated by its reactions with NO in the early period (within ~15min, RO₂ + HO₂ contributed ~15% of RO₂ loss) and in later periods a significant fraction of RO₂ loss was also contributed by the reaction of RO₂ with HO₂ (Fig. S3), based on the measured NO_x, RO₂, and HO₂ concentrations and their rate constants for the reactions with RO₂ (Jenkin et al., 1997; Jenkin et al., 2019). At high NO, the RO₂ fate was by far dominated by the RO₂+NO reaction.

2.2 Characterization of HOM

HOM were characterized by a Chemical Ionization time-of-flight Mass Spectrometer (CIMS, Aerodyne Research Inc., USA) with nitrate (¹⁵NO₃⁻) as the reagent ion, which has a mass resolution of ~4000 (m/dm). The details of the instrument are described in previous publications (Pullinen et al., 2020; Mentel et al., 2015; Ehn et al., 2014). Briefly, ¹⁵NO₃⁻ produced from ¹⁵N nitric acid, was used as the reagent ion to distinguish complexation with the reagent ion from NO₃ groups in target molecules. NO₃⁻-CIMS is suitable for detecting oxygenated organic compounds with high oxygen number. The mass spectra were analysed by Tofware (version 2.5.7, Tofwerk/Aerodyne) in Igor Pro (version 6.37 WaveMetrics, Inc.). In this study, the mass spectra of HOM products during the first 15 min after louvres opening were analysed because the particle number concentration (<30 #/cm⁻³) remained low in the initial phase of the reaction. After attributing molecular formulas of HOM to different m/z, their concentrations were calculated using the calibration coefficient of H₂SO₄ (C: 2.5×10¹⁰ molecule·cm⁻³·nc⁻¹) as described before (Zhao et al., 2021; Pullinen et al., 2020), where the charge efficiency of HOM and H₂SO₄ was assumed to be close to the collision limit (Pullinen et al., 2020; Ehn et al., 2014). The details of the calibration with H₂SO₄ were described in Supplement Sect. S1. The loss of HOM was corrected by using a wall loss rate of 2.2×10⁻³ s⁻¹ in fan-on condition and ~6.0×10⁻⁴ s⁻¹ in fan-off condition as quantified previously (Guo et al., 2022; Zhao et al., 2018a), and a dilution loss rate ~1×10⁻⁶ s⁻¹ (Zhao et al., 2015b). For details, we refer to these latter publications; briefly, the wall loss rate of HOM in our chamber

was estimated as that of the decay of organic vapor (such as $C_{10}H_{15}NO_{9-12}$ (nitrated compounds) and $C_{10}H_{14}O_{8-11}$ (non-nitrated compounds) in the reaction of limonene with OH in the presence of NO) concentrations in the dark (Guo et al., 2022). Overall, wall loss correction and dilution correction only affect the HOM yield by ~5.8% and <1%, respectively.

2.3 Data analysis

The HOM yield was obtained using the concentration of the HOM, divided by the concentration of limonene consumed by OH, which is the dominant oxidant of limonene and accounts for over 99% of limonene loss rate. HOM yield was calculated over the first 15 min after louvres opening as followed:

$$Y = \frac{[HOM]}{\Delta[VOC]_r} = \frac{I_{HOM} * C}{\Delta[VOC]_r} \quad (\text{Eq. 1})$$

where $[HOM]$ means the concentrations of total HOM corrected for wall loss and dilution loss, $\Delta[VOC]_r$ is the consumption concentrations of limonene corrected for wall loss and dilution loss, I_{HOM} is the total signal intensity of HOM normalized to the total signal, and C is the calibration coefficient of H_2SO_4 . The calibration and wall loss and dilution loss correction are described in detail in the Supplement (S1).

Based on the C_{10} closed-shell products from unimolecular and bimolecular reactions of the C_{10} peroxy radical families $C_{10}H_{15}O_x^\bullet$ and $C_{10}H_{17}O_x^\bullet$, $C_{10}H_{16}O_x$ can be divided into carbonyls ($R=O$) and epoxides from $C_{10}H_{17}O_x^\bullet$, as well as alcohols (ROH) and hydroperoxides (ROOH) from $C_{10}H_{15}O_x^\bullet$. The contribution of $C_{10}H_{17}O_x^\bullet$ -related products to $C_{10}H_{16}O_x$, was quantified as follows. For a HOM- RO_2 , the production rate of alcohols (ROH) can be obtained according to R2.

$$\frac{d[ROH]}{dt} = \alpha k_{RO_2+RO_2} [RO_2] [RO_2]^T \quad (\text{Eq.2})$$

The production rate of hydroperoxides (ROOH) can be obtained according to R1 a, which forms ROOH with a yield β , where β is close to 1 for most RO_2 (Jenkin et al., 2019).

$$\frac{d[ROOH]}{dt} = k_{RO_2+HO_2} [RO_2] [HO_2] \beta \quad (\text{Eq.3})$$

The production rate of carbonyls ($R=O$) can be obtained according to R2 and R6.

$$\frac{d[R=O]}{dt} = (1 - \alpha) k_{RO_2+RO_2} [RO_2] [RO_2]^T + k_{uni} [RO_2] \quad (\text{Eq.4})$$

Combing Eq.2-4, one can get Eq. 5:

$$\begin{aligned} \frac{\frac{d[ROH]}{dt} + \frac{d[ROOH]}{dt}}{\frac{d[R=O]}{dt}} &= \frac{\alpha k_{RO_2+RO_2} [RO_2] [RO_2]^T + k_{RO_2+HO_2} [RO_2] [HO_2] \beta}{(1 - \alpha) k_{RO_2+RO_2} [RO_2] [RO_2]^T + k_{uni} [RO_2]} \\ &= \frac{\alpha k_{RO_2+RO_2} [RO_2]^T + k_{RO_2+HO_2} [HO_2] \beta}{(1 - \alpha) k_{RO_2+RO_2} [RO_2]^T + k_{uni}} \end{aligned} \quad (\text{Eq. 5})$$

where $[RO_2]^T$ and $[HO_2]$ are the total concentrations of RO_2 and the concentration of HO_2 in the reaction system, respectively. k_{uni} , $k_{RO_2+RO_2}$ and $k_{RO_2+HO_2}$ represent the rate coefficient of the unimolecular termination of RO_2 and the bimolecular reactions of RO_2 with RO_2 and HO_2 . α and $1-\alpha$ are the carbonyl yield and the alcohol yield in reactions of $RO_2 + RO_2$, respectively. Wall loss was neglected due to its minor effects on the concentrations of the products (~5.8%).

For $C_{10}H_{15}O_x^\bullet$ family, the Eq. 5 is equivalent to Eq. 6:

$$\frac{\frac{d[ROH]}{dt} + \frac{d[ROOH]}{dt}}{\frac{d[R=O]}{dt}} \Bigg|_{C_{10}H_{15}O_x^\bullet} = \frac{d[C_{10}H_{16}O_x]_{ROH+ROOH}}{d[C_{10}H_{14}O_x]} = \frac{d[C_{10}H_{16}O_x] \times (1-[R=O])\%}{d[C_{10}H_{14}O_x]} \quad (\text{Eq. 6})$$

For $C_{10}H_{17}O_x^\bullet$ family, the Eq. 5 is equivalent to Eq. 7:

$$\frac{\frac{d[ROH]}{dt} + \frac{d[ROOH]}{dt}}{\frac{d[R=O]}{dt}} \Bigg|_{C_{10}H_{17}O_x^\bullet} = \frac{d[C_{10}H_{18}O_x]}{d[C_{10}H_{16}O_x]_{R=O}} = \frac{d[C_{10}H_{18}O_x]}{d[C_{10}H_{16}O_x] \times [R=O]\%} \quad (\text{Eq. 7})$$

As shown in the Eq. 2, we assume the same k_{uni} , $k_{\text{RO}_2+\text{RO}_2}$, $k_{\text{RO}_2+\text{HO}_2}$, α and β for a given $\text{C}_{10}\text{H}_{15}\text{O}_x\cdot$ and $\text{C}_{10}\text{H}_{17}\text{O}_x\cdot$ family. Consequently, the ratios of $\frac{d[\text{ROH}]+d[\text{ROOH}]}{d[\text{R=O}]}$ for $\text{C}_{10}\text{H}_{15}\text{O}_x\cdot$ and $\text{C}_{10}\text{H}_{17}\text{O}_x\cdot$ are the same. Eq. 8 can then be derived from Eq. 6 and 7, to yield $[\text{R=O}]\%$, which represents the contribution of the carbonyls produced from $\text{C}_{10}\text{H}_{17}\text{O}_x\cdot$ to $\text{C}_{10}\text{H}_{16}\text{O}_x$.

$$\frac{d[\text{C}_{10}\text{H}_{16}\text{O}_x]\times(1-[\text{R=O}]\%)}{d[\text{C}_{10}\text{H}_{14}\text{O}_x]} = \frac{d[\text{C}_{10}\text{H}_{18}\text{O}_x]}{d[\text{C}_{10}\text{H}_{16}\text{O}_x]\times[\text{R=O}]\%} \quad (\text{Eq. 8})$$

205 Based on this, about 90.1% and 98.8% of $\text{C}_{10}\text{H}_{16}\text{O}_x$ were estimated to be carbonyls from $\text{C}_{10}\text{H}_{17}\text{O}_x\cdot$ at low and high NO, respectively. We did a sensitivity analysis to test the influence of varying the k_{uni} , $k_{\text{RO}_2+\text{RO}_2}$, $k_{\text{RO}_2+\text{HO}_2}$, and α using the ranges of these parameters reported in the literature on the fraction of carbonyl in $\text{C}_{10}\text{H}_{16}\text{O}_x$ and on the importance of H-abstraction channel in HOM formation. When k_{uni} , $k_{\text{RO}_2+\text{RO}_2}$, $k_{\text{RO}_2+\text{HO}_2}$, and α were varied in the range of $(0.01-1)\times 10^{-12} \text{ cm}^3 \text{ molecule}^{-1} \text{ s}^{-1}$, $(0.001-1)\times 10^{-10} \text{ cm}^3 \text{ molecule}^{-1} \text{ s}^{-1}$, $(0.5-2)\times 10^{-11} \text{ cm}^3 \text{ molecule}^{-1} \text{ s}^{-1}$ based on the values in the literature (Crouse et al., 2013; Berndt et al., 2018; Ziemann and Atkinson, 2012), and 0.5, respectively, one can get the yield of carbonyl according to Eq. 6 and Eq. 7, which ranged from 90%-96% at low NO and 97%-100% at high NO. This indicated that the yields of carbonyl are not sensitive to these assumption of k and α .

2.4 Theoretical kinetic study of $\text{C}_{10}\text{H}_{15}\text{O}$ alkoxy and $\text{C}_{10}\text{H}_{15}\text{O}_2$ peroxy radicals

The formation mechanism of $\text{C}_{10}\text{H}_{15}\text{O}$ alkoxy and $\text{C}_{10}\text{H}_{15}\text{O}_2$ peroxy radicals were considered in the theoretical kinetic study. The geometries of the intermediates and transition states for the first steps in the mechanism were first optimized using the M06-2X/cc-pVDZ methodology (Zhao and Truhlar, 2008; Dunning, 1989), with an exhaustive characterization of all conformers for each reactant and transition state. All geometries obtained thus were further optimized at the M06-2X-D3/aug-cc-pVTZ level of theory which includes D3 diffusion corrections (Goerigk et al., 2017; Grimme et al., 2011). Moments of inertia for molecular rotation, and wavenumbers for vibration were obtained at the same level of theory, with a vibrational scaling factor of 0.971 (Alecú et al., 2010; Dunning, 1989). The barrier heights were further improved by single-point calculations at the CCSD(T)/aug-cc-pVTZ level of theory (Dunning et al., 2001; Bartlett and Purvis, 1978) (all T1 diagnostics ≤ 0.029). The expected uncertainty on the reaction barrier heights at this level of theory is $\pm 0.5 \text{ kcal mol}^{-1}$. All quantum chemical calculations were performed using the Gaussian-16 software suite (Frisch et al., 2016). The quantum chemical data underlying the theoretical kinetic calculations is provided in the supplement.

225 The rate coefficients for the individual reactions at the high-pressure limit were then calculated using multi-conformer transition state theory, MC-TST (Vereecken and Peeters, 2003), incorporating the data for all conformers obtained as described above. Tunnelling is accounted for using an asymmetric Eckart barrier correction (Johnston and Hecklen, 1962; Eckart, 1930). Based on earlier work at a similar level of theory in comparison with experimental data on H-migration in $\text{RO}_2\cdot$ radicals with no or only one oxygenated functionality (Vereecken and Nozière, 2020; Nozière and Vereecken, 2019) and available theoretical literature data on ring closure reactions (Vereecken et al., 2021), we estimate the thermal rates to be accurate to a factor 2 to 3.

2.5 SAR-based mechanism development for autoxidation

The kinetics of the chemistry following the ring breaking is expected to be fairly well described based on structure-activity relationships (SARs), and no explicit theoretical kinetic calculations were performed. We employ the same approach for deducing the mechanism as described in our recent work (Shen et al., 2022). Briefly, we only take into account a limited oxidation network by considering all possible reaction channels and select only the dominant channels, based on their rate as predicted by SARs. For the rate coefficients for most H-migrations in $\text{RO}_2\cdot$ radicals, we base ourselves on the SAR by Vereecken and Nozière (2020); this SAR was reported to reproduce the scarce experimental data within a factor of 2, but for multi-functionalized species such as studied in this work the scatter on the data within each SAR category reaches an order of magnitude. For H-migrations in cycloperoxides, we additionally rely on the systematic study by Vereecken et al. (2021), who

explicitly calculated rate coefficients for peroxy radicals formed after RO₂• ring closure reactions. For those reaction classes that are not covered by either SAR, we estimate a rate by extrapolating the reactivity trends in the SARs, albeit with a large uncertainty. For ring closure reactions in unsaturated RO₂• we employ on the SAR by Vereecken et al. (2021), where it is assumed that the presence of another cycloperoxide ring does not influence the rate. In assessing the fate of an RO₂• radical with one or more -OOH groups, we account for the possibility of H-atom scrambling, as described extensively in the literature (Praske et al., 2019; Møller et al., 2019; Jørgensen et al., 2016; Nozière and Vereecken, 2019; Knap and Jørgensen, 2017). These fast H-migrations between the -OO• and -OOH groups are typically much faster than other unimolecular channels, leading to a fast equilibration among all accessible OOH-substituted RO₂• radicals, and the dominant reaction is chosen among those available to the pool of RO₂• radicals. We refer to Vereecken and Nozière (2020) for a more detailed description of this feature. In the early stages of the oxidation, we also use the recent work by Piletic and Kleindienst (2022). Finally, for alkoxy radical chemistry, we employ the SARs for decomposition and H-migration by Novelli et al. (2021) and Vereecken and Peeters (2009, 2010). For hydroperoxyl-substituted alkoxy radicals we note explicitly that H-migration of the hydroperoxide H-atom, forming an alcohol and an RO₂ radical, is typically very fast, $k(298\text{ K}) \geq 10^{10}\text{ s}^{-1}$ (Vereecken and Nozière, 2020), and is often the most likely loss process in later alkoxy stages in the autoxidation chain. This fast H-migration supports competitive autoxidation even under high-NO conditions despite the formation of alkoxy intermediates that threaten to fragment the molecule.

3 Results and discussion

3.1 Overview of HOM spectra

The mass spectra of gas phase products HOM formed in the oxidation of limonene by OH at two different NO_x levels are demonstrated in the Fig. 1. The HOM products can be classified according their mass to charge ratio (m/z) as either monomers (200-400 Th, including C₆-C₉ monomers and C₁₀ monomers (320-400 Th)) or dimers (480-600 Th, C₁₇-C₂₀ dimers). We did not observe any trimer products (Fig. S4). The signal intensity of monomers is higher than dimers at both low and high NO (Fig. 1 and Fig. 2), where monomers accounted for over 80% of total HOM. Both the signal intensity and the fraction of the observed dimers at high NO were much less than that at low NO (Fig. 1 and Fig. 2). In the following (Sect. 3.2) we discussed product distribution and formation mechanism of monomers and dimers in details.

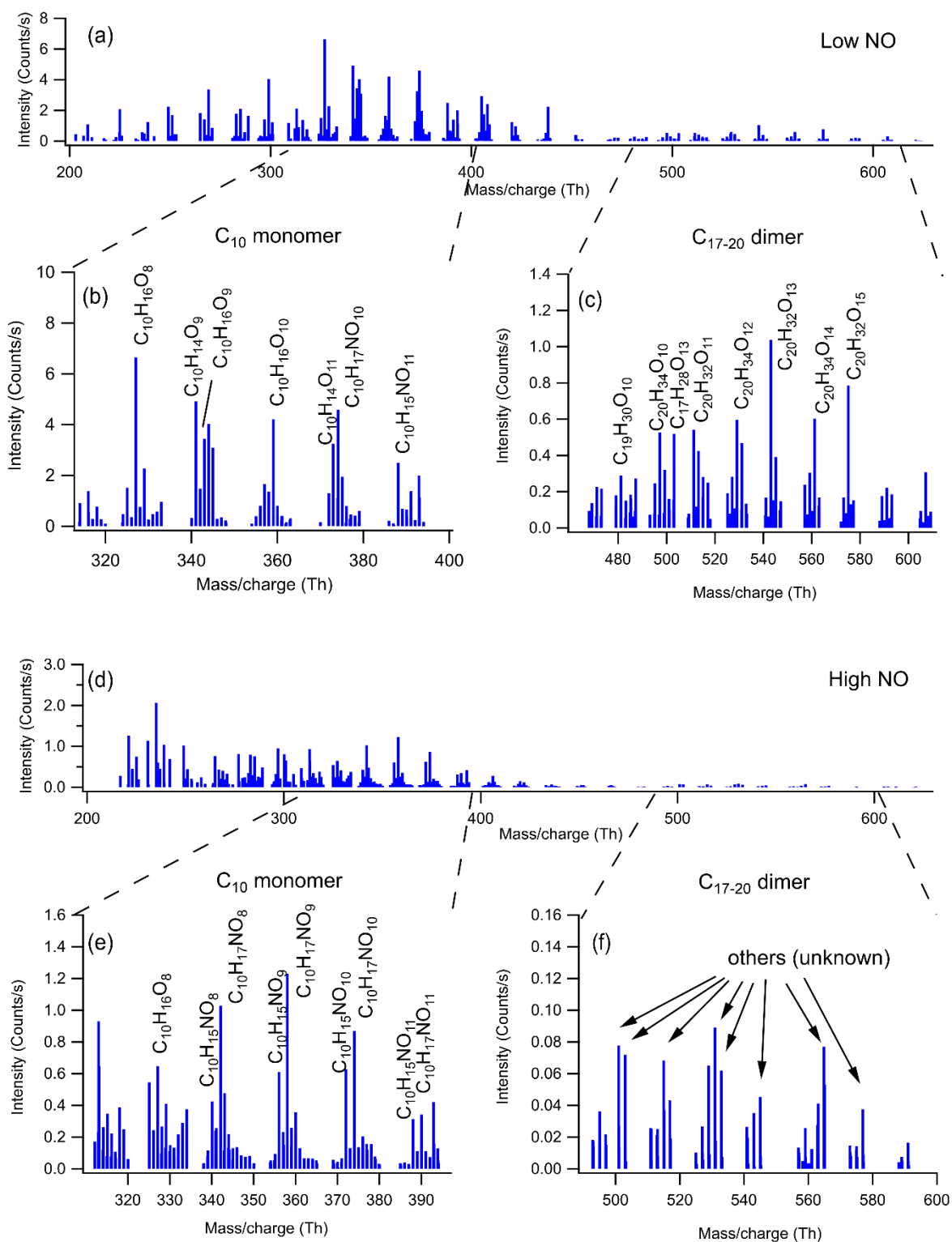


Figure 1. Mass spectrum of the HOM formed in the oxidation of limonene by OH in (a) low and (d) high NO condition. The mass spectra were obtained within 15 min after opening the louvres and were averaged over 15 min. Figure 1 (b, c, e, f) present expanded mass spectra where major peaks are labelled with their molecular formulas.

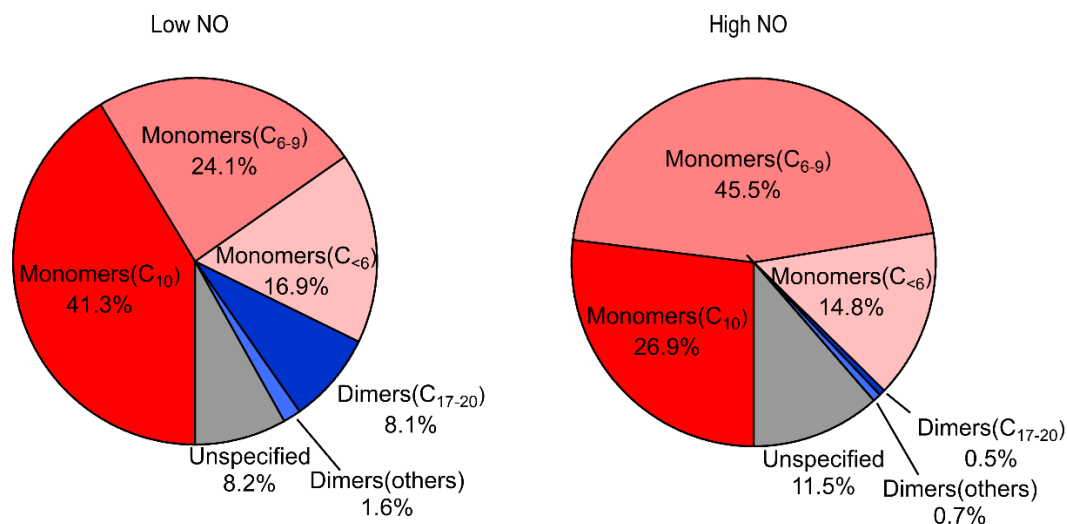


Figure 2. HOM product distribution including monomers (C₁₀, C₆₋₉, C_{<6}), dimers (C₁₇-C₂₀, other), and unspecified species in low and high NO conditions [at the first 15 min of experiments](#).

275

3.2 Identification and formation mechanism of HOM

3.2.1 Overview of HOM monomers

Closed-shell HOM monomers are characterized by repeating pattern of molecular formulas with an increasing number of oxygen atoms in the mass spectrum. The repeating pattern in the mass spectrum at every 16 Th form series of HOM monomer families, such as C₆H_{8/10}O_x, C₆H_{9/11}NO_x, C₇H_{8/10/12}O_x, C₇H_{9/11}NO_x, C₈H_{10/12/14}O_x, C₈H_{11/13}NO_x, C₉H_{12/14/16}O_x, C₉H_{13/15}NO_x, C₁₀H_{14/16/18}O_x, and C₁₀H_{15/17}NO_x (Fig. S5). It is worth noting that some open-shell radicals, such as C₁₀H₁₅O_x•(x=6-15) and C₁₀H₁₇O_x•(x=6-15), were also observed; these are a significant fraction of HOM monomers and will be discussed in detail in section 3.2.2. These open-shell molecules were likely RO₂ radicals, as we are not able to detect the very short lived alkoxy radicals (RO) and alkyl radicals (R). The closed shell products (C_{≤10}H_yO_x and C_{≤10}H_yNO_x) will be discussed in the following from the perspective of RO₂ chemistry, i.e., as termination products of RO₂. It should be noted that each molecular mass can represent several isomers, and that there may be more than one pathway to form a given product; our experiments do not allow to discriminate these and an in-depth discussion is outside the scope of this work.

HOM monomers were classified into C₁₀ and C₆₋₉ monomers according to the numbers of carbon atoms. The abundance of C₆₋₉ monomers (~27.0% combined) was lower than C₁₀ compounds (~46.4%) at low NO. In addition to C₁₀ and C₆₋₉ monomers, other monomers accounted for ~18.9% of all monomers and unspecified monomers accounted for ~7.7%. As shown in Fig. S5, C₆₋₁₀ monomers contain either none or one nitrogen atoms, and a higher fraction of organic nitrates was observed in high NO condition (nitrate HOM: 31% at low NO and 41% at high NO). This is as expected given that the fraction of RO₂ terminated by NO forming organic nitrate was higher at high NO. Higher fractions of organic nitrate have also been observed by the previous studies in the photo-oxidation of other monoterpenes at high NO (Pullinen et al., 2020; Shen et al., 2022).

3.2.2 C₁₀ monomer product distribution

At low and high NO condition, C₁₀ compounds (C₁₀H₁₄O_x, C₁₀H₁₅NO_x, C₁₀H₁₆O_x, C₁₀H₁₇NO_x and C₁₀H₁₈O_x) were the abundant monomers with a fractional contribution of ~27-~41% (see Fig. 2). In this study, we observed two major RO₂ radical families, C₁₀H₁₅O_x•(x=6-15) and C₁₀H₁₇O_x•(x=6-15), and their corresponding termination products, C₁₀H₁₄O_{x-1}, C₁₀H₁₆O_{x-1}, C₁₀H₁₆O_x, and C₁₀H₁₅NO_{x+1}, and C₁₀H₁₆O_{x-1}, C₁₀H₁₈O_{x-1}, C₁₀H₁₈O_x, and C₁₀H₁₇NO_{x+1} respectively, which contained carbonyl, hydroxyl, hydroperoxyl and nitrate, respectively (see Fig. 3, Fig. S5, Table S2, Table S3, Table S6, and Table S7). C₁₀H₁₄O_x and C₁₀H₁₆O_x

300

were likely carbonyl compounds formed via unimolecular termination of $C_{10}H_{15}O_x\cdot$ and $C_{10}H_{17}O_x\cdot$, respectively. Overall, at high NO, organic nitrates were the most abundant among all classes of HOM monomers and their relative proportion was much higher than at low NO (Fig. 3). Under low NO condition, $C_{10}H_{14}O_x$ and $C_{10}H_{16}O_x$ family are the two most abundant family among C_{10} monomers. This is similar to the C_{10} monomers products from photooxidation of α -pinene by OH radical (Shen et al., 2022). The NO_x dependence for $C_{10}H_{15}O_x\cdot/C_{10}H_{17}O_x\cdot$ may be attributed to the differences in their reactivity. One explanation to the NO_x dependence is that the autooxidation of $C_{10}H_{15}O_x\cdot RO_2$ radicals may be faster than that of $C_{10}H_{17}O_x\cdot RO_2$ radicals, which leads to the lower concentration of $C_{10}H_{15}O_x\cdot$ measured in this study and higher sensitivity to NO concentrations. Based on the measured concentrations of $RO_2\cdot$, $HO_2\cdot$, and NO, an average bimolecular $RO_2\cdot$ loss rate of $\sim 0.02 s^{-1}$ (low NO) and $\sim 3.5 s^{-1}$ (high NO) was estimated in our previous study (Zhao et al., 2018), which is predominately due to the reaction with NO. From this, we infer that the average reactive rate of $C_{10}H_{17}O_x\cdot$ at high NO is higher than that at low NO, which finally result in the increases of $C_{10}H_{17}O_x\cdot$ consumption. This inference is supported by the higher relative contribution of $C_{10}H_{17}NO_x$ at high NO (36.3%) than at low NO (16.1%) in Fig. 2. When we focus on the first 15 min of experiments to avoid the influence of secondary chemistry, ratios of $C_{10}H_{16}O_x(R-OH/OOH)/C_{10}H_{15}O_x\cdot$ can be derived of 0.47 and 0.02 at low and high NO, respectively. The ratio of $C_{10}H_{18}O_x/C_{10}H_{17}O_x\cdot$ at low NO (0.38) is higher than at high NO (0.1). The decrease of $C_{10}H_{16}O_x(R-OH/OOH)/C_{10}H_{15}O_x\cdot$ at high NO compared to low NO was more evident than the decrease of $C_{10}H_{18}O_x/C_{10}H_{17}O_x\cdot$. Theoretically, though, they should be similar. The difference may be attributed to the shift in $C_{10}H_{15}O_x\cdot$ distribution with different number of O, as evident in Fig. S6, and different isomers at high NO compared to low NO. At high NO there might thus be more $C_{10}H_{15}O_x\cdot$ that react slower with HO_2 or have a lower branching ratio forming ROOH in RO_2+HO_2 , which depends on the explicit RO_2 structure, or have a lower yield forming ROH in RO_2+RO_2 .

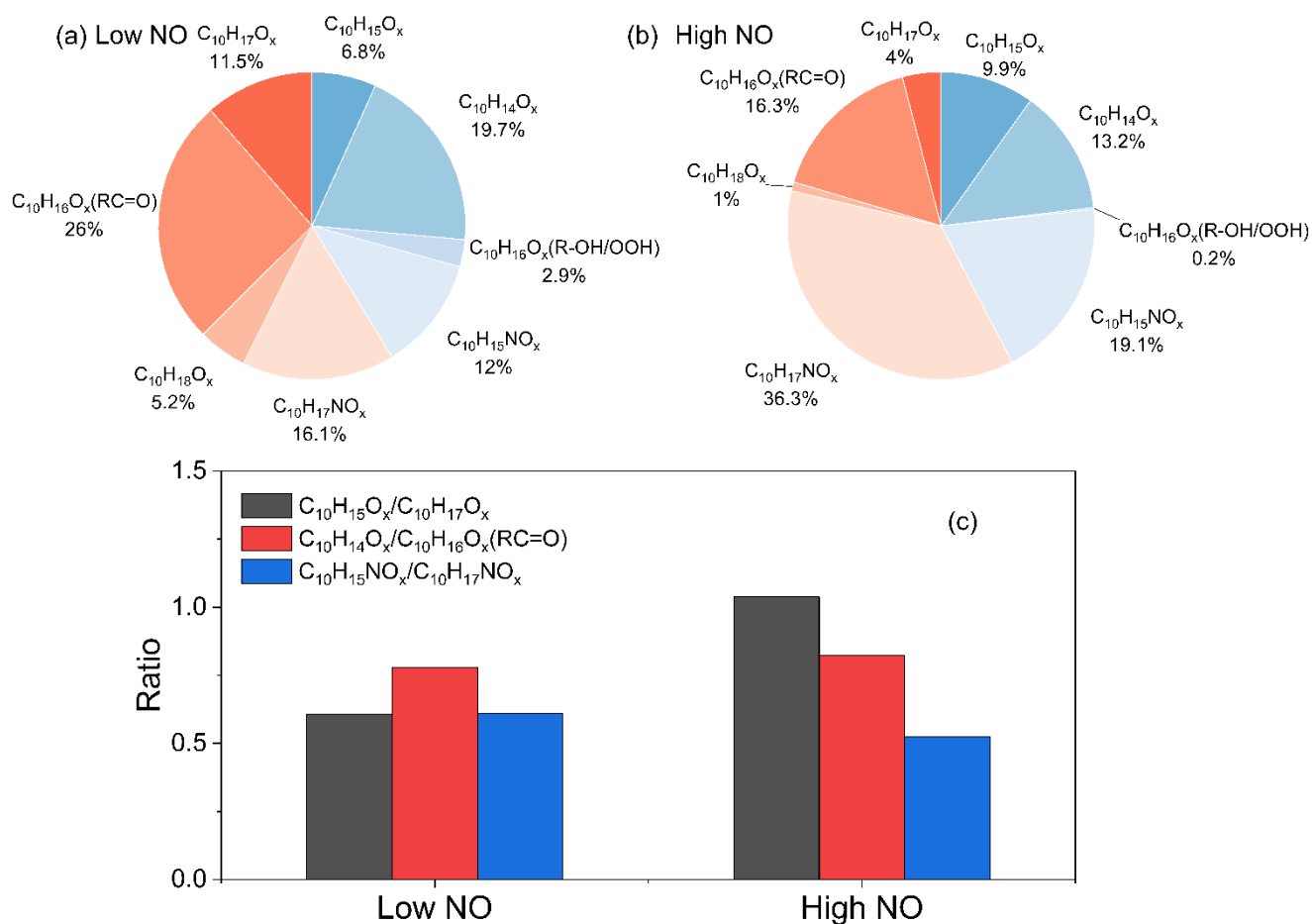


Figure 3. Product distribution within C_{10} monomers at (a) low and (b) high NO and (c) the ratio of $C_{10}H_{15}O_x\cdot$ to $C_{10}H_{17}O_x\cdot$ and of their termination products. As in Fig.2, data of the first 15 min of the experiments were used.

325 3.2.3 Monomers with C_{<10} monomers and dimers

A number of monomers with carbon number less than 10 (C_{<10}) were observed in this study. The monomers (C_{<10}) account for about 24.1-45.5% of the total monomers. The two radicals C₇H₉O_x• and C₇H₁₁O_x• were likely produced from C₁₀H₁₅O_x• radicals and C₁₀H₁₇O_x• radicals, respectively (see below). The ratios of total termination products from C₇H₉O_x• to those from C₇H₁₁O_x• are 0.7 at both low and high NO, which is generally consistent with the ratio of C₁₀H₁₅O_x• radicals and C₁₀H₁₇O_x• radicals for C₁₀-related products. This suggests that chemistry related to C₁₀H₁₅O_x• radicals plays a significant role in formation of C_{<10} monomers. Although the concentrations of monomers (C_{<10}) are smaller than of C₁₀ monomers, they may also contribute to the formation of dimers, which further condense onto particles.

We observed a number of dimer families, including C₂₀H₃₀O_x (x=10,12-18), C₂₀H₃₂O_x (x=9-18), C₂₀H₃₄O_x (x=10-17), C₁₉H₃₂O_x (x=10-15), C₁₉H₃₁NO_x (x=11-18), C₁₉H₃₀O_x (x=10-17), C₁₈H₃₀O_x (x=10-14), C₁₉H₂₈O_x (x=11-15), C₁₇H₂₆O_x (x=11-15), C₁₇H₂₄O_x (x=12-17) in low NO condition, and C₂₀H₃₀O_x (x=12-16), C₂₀H₃₂O_x (x=11-18), C₂₀H₃₄O_x (x=10-15), C₁₉H₂₈O_x (x=11-17), C₁₇H₂₆O_x (x=12-15) in high NO condition (see Table S4 and Table S5). Compared to monomers, the peak intensity of dimers both at low and high NO conditions are much lower (Fig. S7 and Fig. S8). Furthermore, the peak intensity of dimers in low NO condition is higher than that in high NO condition. This inhibitory effect of NO_x in dimer formation is consistent with the phenomenon described in previous studies (Pullinen et al., 2020; Yan et al., 2016; Shen et al., 2022). In the following discussion we will focus on C₁₀ monomers. However, more information on C_{<10} monomers and dimers can be found in Supplement Sect. S2.

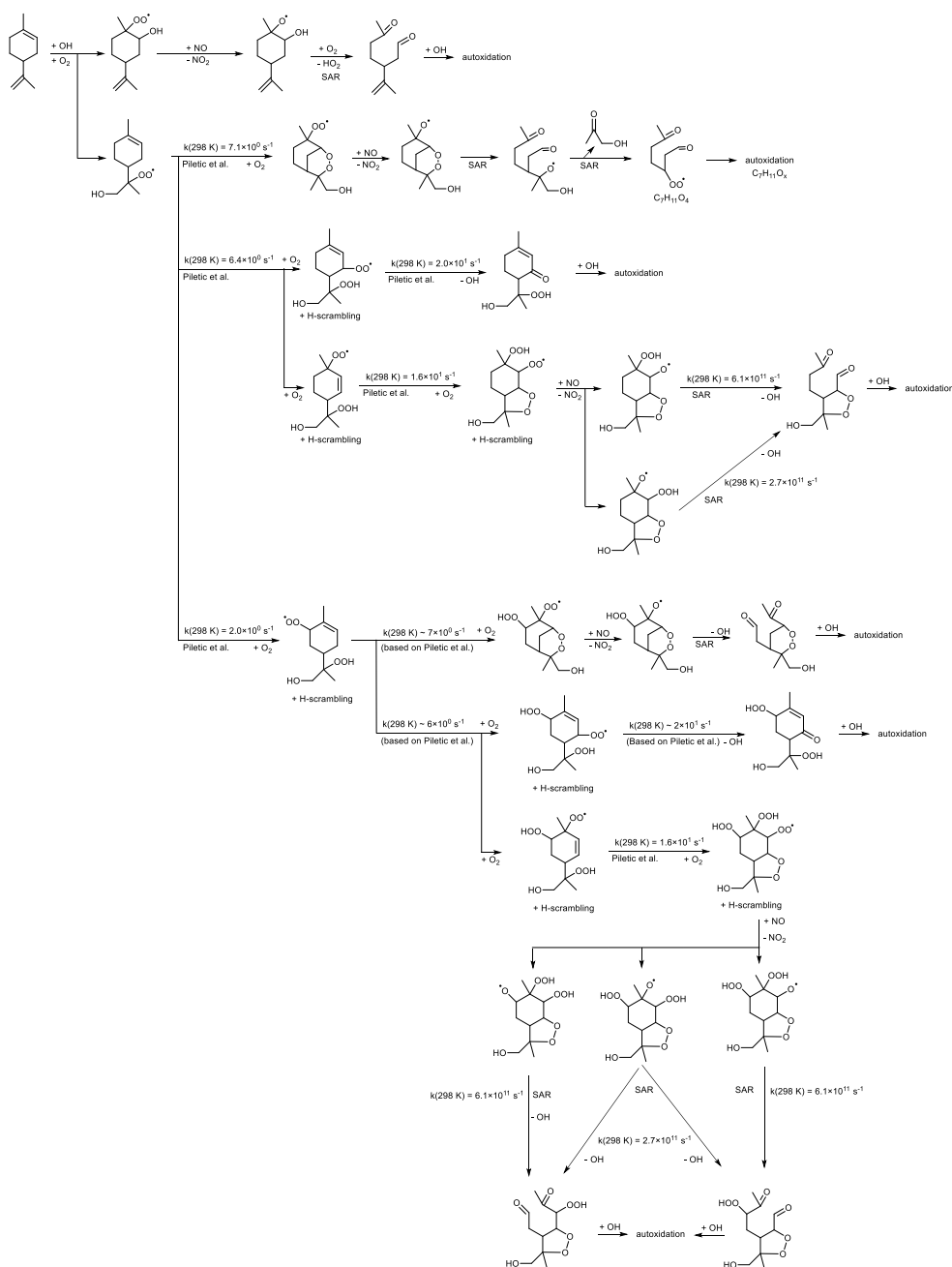
3.3 Formation pathways of HOM monomers

In this section we discuss potential formation pathways for C₁₀ monomers. These pathways are tentative only, and are based on the current knowledge on autoxidation as represented in various SARs, where we examine only those paths estimated as being the fastest. Our observations do not distinguish between different isomers and we cannot validate the reaction scheme. We also observed HOM with only 7, 8 or 9 carbon atoms and their possible formation pathways, involving a fragmentation step in an intermediate alkoxy radical, are inspected in the supporting information (see schemes S1 and S2).

3.3.1 HOM from OH addition

The C₁₀H₁₇O_x• radicals are formed from the OH addition reaction of limonene and subsequent autoxidation (see Table S3). Scheme 1 shows possible oxidation routes for the OH addition to both double bonds, considering the particular channels leading to tertiary alkyl radicals and depicting the most likely reactions as estimated based on theoretical work and SARs (Peeters et al., 1999; Vereecken et al., 2007; Jenkin et al., 2018). The C₁₀H₁₇O₃• RO₂ radical formed after O₂ addition on the OH adducts has access to a wide range of reactions, but in most cases the six-membered ring is retained in the first RO₂ steps, leading to slow autoxidation steps (Vereecken et al. 2021). This allows the reaction with NO to become important, whereafter the decomposition of a β-OH or β-OOH alkoxy radical leads to carbonyl formation and thus chain termination. This analysis suggests that HOM formation after OH addition either proceeds through less favourable pathways or involves secondary chemistry. The complete explicit mechanism is highly branched and complex, and missing pathways in Scheme 1 could together contribute to sizable HOM formation. Furthermore, the rate estimates are tentative, with uncertainties of an order of magnitude or more, so we cannot exclude that primary HOM formation is possible and important. The primary products predicted in Scheme 1 (or formed through similar termination reactions in other channels) can react again with OH, initiating secondary autoxidation. Most of these products have the six-membered ring broken, and should be more amenable to further autoxidation steps and thus readily yield HOM. However, this extra bimolecular OH reaction takes time, and can delay formation of HOM. An analysis of the secondary chemistry is outside the scope of this work, and at this time we do not propose a reaction scheme that covers the full range of C₁₀H₁₇O_x• radicals and related products observed.

365 In our previous study, the average bimolecular RO₂ loss rate was estimated at ~0.02 s⁻¹ (low NO) and ~3.5 s⁻¹ (high NO) (Zhao et al., 2018a). In both cases RO₂ loss is due predominantly to the reaction with NO (see Fig. S3), which leads to the organic nitrate termination products, as illustrated in Fig. 3. Even at low NO with ~0.2 ppb, organic nitrates contribute a large portion of HOM (33%). The relevant termination products from C₁₀H₁₇O_x• (x=8-13) in reactions with HO₂ and RO₂ are identified as C₁₀H₁₈O_x, C₁₀H₁₈O_{x-1}, and C₁₀H₁₆O_{x-1}. However, C₁₀H₁₈O_x accounted for only 5.2% and 1% in C₁₀ monomers at 370 low and high NO, respectively, as in high NO conditions these loss processes are overwhelmed by the RO₂ + NO reaction.



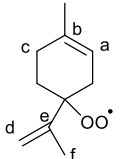
375 **Scheme 1.** Example reaction scheme for C₁₀H₁₇O_x• RO₂ formation after OH-addition in limonene, based on the most likely reactions predicted in theoretical work and SAR predictions. All RO₂ intermediates have competing reactions (not shown) under current conditions with HO₂ (forming hydroperoxides) and NO (forming alkoxy and nitrates).

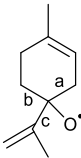
3.3.2 HOM from H-abstraction by OH

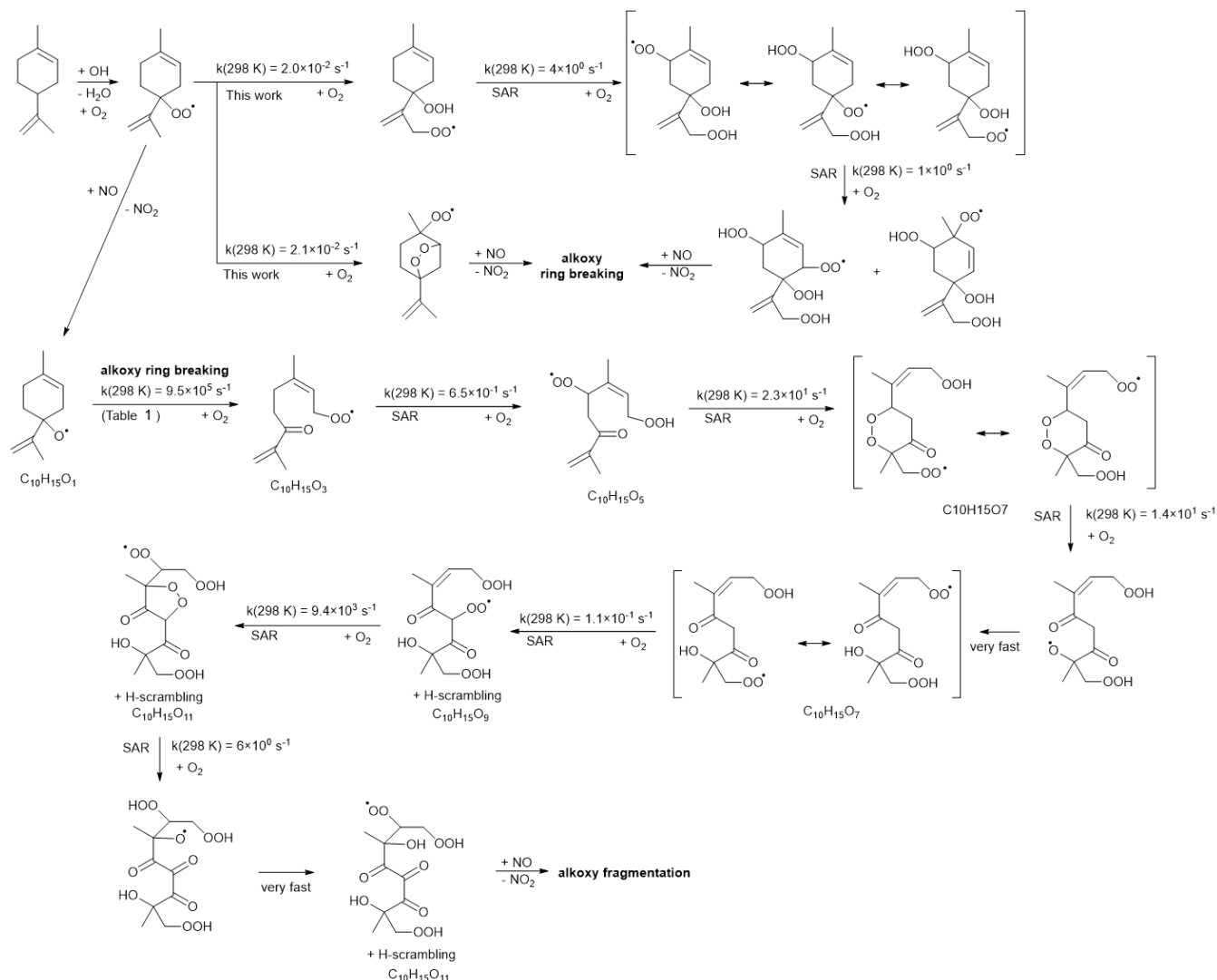
The observed C₁₀H₁₅O_x• radicals mainly originate from an H-abstraction reaction by OH, removing one of the limonene H-atoms. In principle, C₁₀H₁₅O_x• peroxy radicals might also form through secondary chemistry of first-generation C₁₀ oxidation

380 products of the limonene+OH reaction. The limonaldehyde ($C_{10}H_{16}O_2$) is the most abundant (99%) first-generation C_{10} product reported in limonene+OH reaction (Hakola et al., 1994; Larsen et al., 2001), which can form $C_{10}H_{15}O_4^*$ and the $C_{10}H_{15}O_x^*$ family by further autoxidation through H-abstraction and subsequent O_2 addition. Therefore, we take limonaldehyde into account as the most competitive candidate. For the early stages of our experiments (first 15 min), however, we find that secondary chemistry is not important (Section S2 and Fig. S9 in Supplement). An example pathway for $C_{10}H_{15}O_x^*$ RO_2 radical formation is shown in Scheme 2, based on the most facile H-abstraction channel from limonene. Direct autoxidation of the nascent RO_2 is slow, $k \sim 10^{-2} s^{-1}$, and formation of an alkoxy radical is to be expected immediately or after very few autoxidation steps, especially in high NO conditions. Once the ring structure is broken, fast autoxidation steps are accessible. All RO_2 intermediates have competing reactions (not shown) under current conditions with HO_2 (forming hydroperoxides) and NO (forming alkoxy radicals and nitrates). Alkoxy radicals formed thus can fragment, or continue autoxidation after ring breaking or fast migration of an hydroperoxide H-atom, forming a wider variety of HOM. The nascent peroxy radical formed after H-abstraction of the allylic tertiary H-atom in limonene is not amenable to efficient autoxidation and HOM formation, due to the geometric constraints in the ring. Theoretical kinetic calculations (see Table 1) show that the fastest autoxidation steps occur at rates of $\sim 2 \times 10^{-2} s^{-1}$, i.e., of similar magnitude as the RO_2 loss with NO in the low-NO experiments, but negligible against the $RO_2 + NO$ rate at high NO. Our rate predictions agree with the recent theoretical study by Piletic and Kleindienst (2022). Further autoxidation steps with the ring structure intact are expected to be unfavourable, as well as autoxidation initiated through other H-abstraction sites (Vereecken et al., 2021; Piletic and Kleindienst, 2022). The reaction of the primary RO_2 with NO, however, leads to an alkoxy radical that is most likely to break the six-membered ring, with a total rate coefficient exceeding $\sim 10^6 s^{-1}$ (see Table 1). This alkoxy-peroxy autoxidation step thus removes the geometric constraint, and fast autoxidation reactions become accessible, with rates enhanced by the presence of the double bonds (Vereecken and Nozière, 2020; Møller et al., 2019). Though further alkoxy-peroxy steps are not necessary for HOM formation from limonene, subsequent autoxidation steps will compete against bimolecular reactions with NO, suggesting that more alkoxy-peroxy steps may occur even when the unimolecular lifetime of these later non-cyclic RO_2 radicals is typically shorter than that of the early-stage cyclic RO_2 . Some of these alkoxy intermediates will preferentially break the carbon backbone, leading to fragmentation, while other alkoxy radicals will proceed by H-migration and continue the autoxidation chain. In the latter case, autoxidation then no longer follows the systematic series of adding 2 O-atoms per autoxidation step, and the $C_{10}H_{15}O_x^*$ formation mechanism can proceed both by even-numbered and odd-numbered oxygen numbers x. At high NO concentrations, formation of alkoxy radicals becomes more likely, and thus fragmentation can become more prominent, reducing the yield of $C_{10}H_{15}O_x^*$ related HOM. This is in agreement with the current observations, where more fragment $C_{<10}$ monomers (47.2% in total monomers) are observed at high NO, than at low NO (27.0 %). Further autoxidation of the fragments is also possible, leading to $C_{<10}$ monomers and dimer formation, as discussed in the supplement. The need of a ring-breaking alkoxy-peroxy step in the proposed HOM formation mechanism does suggest that the highest yields of limonene HOM formation may occur at slightly higher NO concentrations than for non-cyclic VOCs who autoxidize even without alkoxy steps.

415 **Table 1.** H-migration, ring closure and C-C bond scission reactions in RO_2^* and RO^* radicals formed from limonene H-abstraction, listing barrier heights E_b (kcal mol⁻¹), rate coefficient k at 298 K (s^{-1}), and parameters for a Kooij equation fit $k(T) = A \times T^n \times \exp(-E_a/T)$ for the temperature range 200-450 K, calculated using the CCSD(T)//M06-2X-D3 level of theory.

RO_2^*	Reaction type	E_b	$k(298K)$	A / s^{-1}	n	E_a / K
	5-Ring closure (a)	19.0	2.1×10^{-2}	$5.40E+07$	1.40	8840
	6-Ring closure (b)	20.2	1.8×10^{-3}	$6.35E+07$	1.27	9390
	Allyl-1,5-H-shift (c)	24.4	1.2×10^{-3}	$6.45E-91$	32.94	-3977
	4-Ring closure (d)	26.9	2.4×10^{-8}	$2.50E+03$	2.79	12292
	5-Ring closure (e)	29.8	2.3×10^{-10}	$1.04E+03$	2.83	13489
	Allyl-1,5-H-shift (f)	22.5	2.0×10^{-2}	$8.68E-81$	29.51	-3667
	Other H-migrations lead to high ring strain and are not competitive					

	Ring opening (a)	9.4	9.5×10^5	7.60E+08	1.42	4409
	Ring opening (b)	10.5	1.6×10^5	1.01E+09	1.39	4972
	Fragmentation (c)	17.4	3.4×10^0	2.49E+09	1.48	8602
	H-migrations or ring closure leads to high ring strain and are not competitive					



420 **Scheme 2.** Example reaction scheme for HOM formation after H-abstraction in limonene, based mostly on SAR prediction and starting at the fastest of 5 allylic H-abstraction sites.

3.3.3 Relative contribution of OH addition versus OH H-abstraction

As $C_{10}H_{15}O_x$ ($x=6-15$) is formed via the OH H-abstraction pathway and $C_{10}H_{17}O_x$ is formed via OH addition, we can compare the relative importance of these two pathways via the ratios of $C_{10}H_{15}O_x$ to $C_{10}H_{17}O_x$ radicals and their termination products.

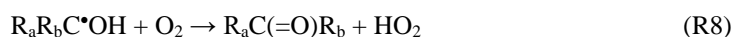
425 At low NO, the ratio of the concentrations of $C_{10}H_{15}O_x$ to $C_{10}H_{17}O_x$ was 0.61 and the ratios of the concentrations of $C_{10}H_{15}O_x$ related termination products carbonyls ($C_{10}H_{14}O_x$) and organic nitrates ($C_{10}H_{15}NO_x$) to $C_{10}H_{17}O_x$ related termination products carbonyls ($C_{10}H_{16}O_x$) and organic nitrates ($C_{10}H_{17}NO_x$) are 0.78 and 0.61, respectively (Fig. 3c). At high NO, the ratio of the concentrations of $C_{10}H_{15}O_x$ to $C_{10}H_{17}O_x$ was ~1.1 (Fig. 3) and the corresponding ratios of the concentrations of $C_{10}H_{15}O_x$ related termination products to $C_{10}H_{17}O_x$ related termination products are 0.82 and 0.53, respectively (Fig. 3c). Note that $C_{10}H_{16}O_x$ can be termination products from either $C_{10}H_{15}O_x$ or $C_{10}H_{17}O_x$ radicals depending on whether they contain hydroxyl/hydroperoxyl (ROH/ROOH) or carbonyl (RC=O) functionalities; the relative substituent contributions in $C_{10}H_{16}O_x$ were quantified using the method described in Sect. 2.2. The concentrations of $C_{10}H_{16}O_x$ and

430

C₁₀H₁₈O_x (alcohol and hydroperoxide products), formed from C₁₀H₁₅O_x• and C₁₀H₁₇O_x• radicals respectively, were found to be negligible, and we can assign C₁₀H₁₆O_x products as carbonyls formed from the OH addition C₁₀H₁₇O_x• radicals. Overall, the C₁₀H₁₅O_x• related products formed via the H-abstraction channel contribute 41% and 42% of C₁₀ HOM monomer respectively at low and high NO.

The ratio between products of C₁₀H₁₅O_x• and C₁₀H₁₇O_x• radicals is stable at both low and high NO (Fig. 4), except for a small decrease at the early reaction times under low NO conditions (Fig. 4c), albeit with large error. At the same time, the nitrate ratio C₁₀H₁₅NO_x/C₁₀H₁₇NO_x is lower than that of C₁₀H₁₄O_x/C₁₀H₁₆O_x, which indicates that carbonyl production from C₁₀H₁₅O_x• is more efficient than from C₁₀H₁₇O_x•. The concentration of peroxy radicals C₁₀H₁₅O_x• and the related termination products C₁₀H₁₄O_x and C₁₀H₁₅NO_x were comparable to C₁₀H₁₇O_x• and its corresponding products, illustrating the significant role of the H-abstraction pathway in the HOM formation from limonene oxidation by OH at low and high NO. The much higher abundance of carbonyl than alcohol is unlikely to be explained by the RO+O₂ forming carbonyl as for large RO (C₁₀ in this study), the RO+O₂ is generally slower than unimolecular reactions including the isomerization (H-shift, i.e., alkoxy-peroxy pathway) and decomposition. The higher abundance of carbonyl products compared to alcohol products indicates that here a large fraction of the carbonyls are not formed from RO₂ + RO₂ reactions (see also Fig. S3), but rather from termination reactions in HOOQOO• radicals eliminating an OH radical after an α-OOH H-atom migration, forming O=QOOH. This observation is in agreement with recent findings for α-pinene (Shen et al., 2022) and previous studies (Miller et al., 2005; Taatjes, 2006; Rissanen et al., 2014; Bianchi et al., 2019).

The large contribution of C₁₀H₁₅O_x• related products to HOM formation can be attributed to the significant contribution of H-abstraction by OH in the initial step. While OH addition is believed to be the major initiation channel in the reaction of limonene+OH and H-abstraction is often ignored in current chemical mechanisms (e.g., MCM v3.3.1), H-abstraction by OH is clearly not negligible. Already previous studies have suggested that H-abstraction can be a significant reaction pathway with ~34±8% branching ratio for the reactions of limonene with OH radical at 298 K (Rio et al., 2010; Dash and Rajakumar, 2015), and 33.6±4.8% at 293 K (Braure et al., 2014). We found that the ratio of C₁₀H₁₅O_x• to C₁₀H₁₇O_x• at high NO condition was higher than 2, emphasizing the importance of H-abstraction. A similar abundance of carbonyls (C₁₀H₁₄O_x) and organic nitrates (C₁₀H₁₅NO_x) stemming from C₁₀H₁₅O_x• radicals compared to their counterparts C₁₀H₁₆O_x and C₁₀H₁₇NO_x from C₁₀H₁₇O_x• at both low and high NO levels (Fig. 3) likewise indicates that H-abstraction in the first step of limonene oxidation by OH is important for the subsequent oxidation. Moreover, the high relative yields of HOM from the H-abstraction channel compared to its contribution in the limonene+OH initiation reaction can be tentatively attributed to the difference in the autoxidation mechanisms (Scheme 1 and 2). Many of the autoxidation channels following OH addition lead efficiently to termination products (Scheme 1) and requires additional OH reactions to undergo further oxidation, whereas the RO₂ formed from H-abstraction readily lend themselves for a sequence of O₂ additions, once the ring structure is broken. The key difference is the presence of β-OH and β-OOH moieties in the alkoxy in the OH addition branch, which can form α-OH alkyl radicals and α-OOH alkyl radicals in fragmentation steps and further lead to HO₂ formation from α-OH alkyl radicals + O₂ (R8) or by regeneration of OH from α-OOH alkyl radicals (R9), thus preventing ring breaking without termination of the autoxidation chain:



In contrast, the alkoxy step after H-abstraction breaks the 6-membered ring to a new RO₂, enhancing autoxidation (scheme 2). The propensity of the RO₂ from OH adducts to terminate the autoxidation chain, especially at higher NO where β-OH and β-OOH alkoxy decomposition is prevalent, then allows the H-abstraction RO₂ to play a more dominant role. Contrary to our earlier studies on β-pinene or limonene with NO₃ (Shen et al., 2021; Guo et al., 2022), where we were able to assign RO₂ and products to first-, second-, or later-generation chemistry, no such clear n-th generation distinction can be made for the HOM mass spectrum traces in the limonene+OH system. This suggests that the observed HOMs are a mixture formed in several

generations of OH-initiation reactions, and lends further credence to our proposal that termination reactions requiring additional OH reactions are hampering the main OH addition channel from efficiently producing HOMs.

To our knowledge, no previous studies have observed $C_{10}H_{15}O_x\bullet$ radicals in limonene oxidation by OH, although in ozonolysis the formation of $C_{10}H_{15}O_x\bullet$ and their termination products including $C_{10}H_{14-16}O_{6-10}$ monomers and $C_{18-20}H_{28-34}O_{6-16}$ was observed (Hammes et al., 2019; Tomaz et al., 2021), and field observations have shown the presence of $C_{10}H_{15}O_x\bullet$ radicals in the atmosphere (Yan et al., 2020; Massoli et al., 2018). Recent theoretical work from Piletic and Kleindienst (2022) concluded that H-abstraction does not contribute to HOM in limonene+OH, but this study did not account for any alkoxy-peroxy autoxidation steps. Our study, then, shows for the first time that H-abstraction significantly contributes to HOM formation in the reaction of limonene+OH under reaction conditions that allow formation of alkoxy radicals such as by reaction with NO, RO₂ or NO₃, as commonly found in the atmosphere.

Currently, an absolute calibration using HOM standards is not possible mainly due to the difficulty to synthesize pure HOM and unclear chemical structures of many HOM. However, we think that it is reasonable to expect a generally similar sensitivity for HOM in this study for the following reasons. First, Hyttinen et al. (2017) found that the increase in binding energy with NO₃⁻ for molecules with an additional hydroxyperoxy group to two hydrogen bond donor functional groups is small for HOM formed in cyclohexene ozonolysis. As HOM in this study generally contain more than two hydrogen bond donor functional groups, their sensitivity is expected to be similar. We used a unified H₂SO₄-based calibration coefficient for HOM, which is commonly used to calibrate NO₃⁻-CIMS (Kirkby et al., 2016; Jokinen et al., 2015; Rissanen et al., 2014; Ehn et al., 2014). Second, although underestimation of certain HOM RO₂ formed from α-pinene+OH reaction has been reported (Berndt et al., 2016), such underestimation was mainly attributed to the steric hinderance in forming HOM-nitrate cluster for HOM with bicyclic structures (C₁₀H₁₇O₇•) and thus not common for all HOM. In our study, we found the significance of C₁₀H₁₅O_x•-related product at all oxygen contents, particularly for closed-shell products with number of oxygen atom great than 8, indicative of more H-donating functional groups (Fig. S6 in revised Supplement). This indicates that the significance of C₁₀H₁₅O_x• related products is not affected by the detection sensitivity, which would mostly affect the sensitivity of less oxygenated compounds. And the presence of NO particularly at high NO leads to ring-opening reactions as shown in Scheme 1. Therefore, the HOM products from OH addition in this study are likely to form stable clusters with nitrate and thus have similar sensitivity with HOM formed via H-abstraction in nitrate CIMS. Third, our previous study showed that using a unified sensitivity of H₂SO₄ only leads to a maximum uncertainty of a factor of two by comparing the condensation HOM and corresponding increase of aerosol mass (Pullinen et al., 2020). If for some currently unknown reason C₁₀H₁₇O_x•-related products had higher sensitivity than C₁₀H₁₅O_x•-related products, this would lead to under-estimate of the significance of OH H-abstraction pathway. This will not change our conclusion that the C₁₀H₁₅O_x• related products contribute significantly to HOM formation.

We have further estimated the uncertainty of fraction of C₁₀H₁₅O_x•-related products in C10-HOM resulted from the allocation of carbonyls and alcohols in C₁₀H₁₆O_x in Eq.2-8. The contributions of C₁₀H₁₅O_x•-related products range from 39.5% to 41.4% at low NO and 42.2% to 42.6% at high NO, respectively. We found that fraction of C₁₀H₁₅O_x• related products in C₁₀-HOM was not much affected by how carbonyls and alcohols in C₁₀H₁₆O_x is allocated.

3.3.4 Comparison against α-pinene HOM formation

In our previous study, we have observed the large contribution of hydrogen abstraction OH to HOM formation in the oxidation of α-pinene by OH (Shen et al., 2022). There, at low NO (0.03-0.1 ppb), the ratio of HOM formed from hydrogen abstraction relative to OH addition increased in the beginning of the experiment and had a delay of 3-5 min before reaching 1:1. At high NO (~17 ppb), an enhancement of the HOM yields formed through H-abstraction was observed, both absolute and relative to the HOM formed through OH addition. Alkoxy radical steps were found to be a prerequisite for the autoxidation and thus

520 HOM formation in the hydrogen abstraction pathway. As discussed in Sect. 3.3.3, in limonene+OH oxidation, the ratios of $C_{10}H_{14}O_x$ to $C_{10}H_{16}O_x$ and of $C_{10}H_{15}NO_x$ to $C_{10}H_{17}NO_x$ and the time series of the ratios were similar at low and high NO. These results indicate that the rate of autoxidation for both the limonene H-abstraction and OH addition channels are affected to a similar extent by competing bimolecular reactions such as with NO. This contrasts with the enhancement of the HOM yield through H-abstraction in the α -pinene system with increasing NO concentrations (Shen et al., 2022).

525 The different kinetic behaviour relative to competing reactions can be attributed to the different molecular structures of α -pinene and limonene. α -pinene is a bicyclic rigid molecule, and the RO_2 formed from H-abstraction do not undergo autoxidation as rate coefficients are $\leq 10^{-4} s^{-1}$ (Shen et al., 2022). Even after breaking the first ring in an alkoxy step, autoxidation rates remain fairly slow, $\leq 10^{-1} s^{-1}$, requiring a second alkoxy step with ring breaking before fast autoxidation occurs. This makes HOM formation through H-abstraction sensitive to the NO concentration in the first few steps. In contrast, limonene has only a single 6-ring and only a single alkoxy ring breaking is needed to allow fast autoxidation in the resulting non-cyclic molecule. Moreover, the primary RO_2 from H-abstraction of limonene can still undergo some slow autoxidation, 530 with rates $\sim 10^{-2} s^{-1}$ (see Table 1), and possibly break the ring at a later stage (see Scheme 2). Overall, then, autoxidation in limonene system after H-abstraction is more competitive even at lower NO than α -pinene system. We should note, though, that the low-NO experiments of limonene oxidation were performed at NO concentrations that were higher by a factor 2 to 7 compared to the low-NO experiment for α -pinene (~ 0.2 ppb and 0.03 - 0.1 ppb, respectively); we speculate that an NO-dependence [of the ratio of HOM formed via H-abstraction versus OH addition](#) might become apparent even in the limonene 535 system at strongly reduced NO levels. The higher absolute contribution of HOM from the H-abstraction channel in limonene (H-abstraction related HOM yields: [0.77%](#) low NO and [0.10%](#) at high NO, shown in Sect. 3.4) is also affected by the higher branching ratio of H-abstraction in limonene+OH, $\sim 34\%$ (Rio et al., 2010; Dash and Rajakumar, 2015), compared to α -pinene+OH, $\sim 11\%$ (Vereecken and Peeters, 2000).

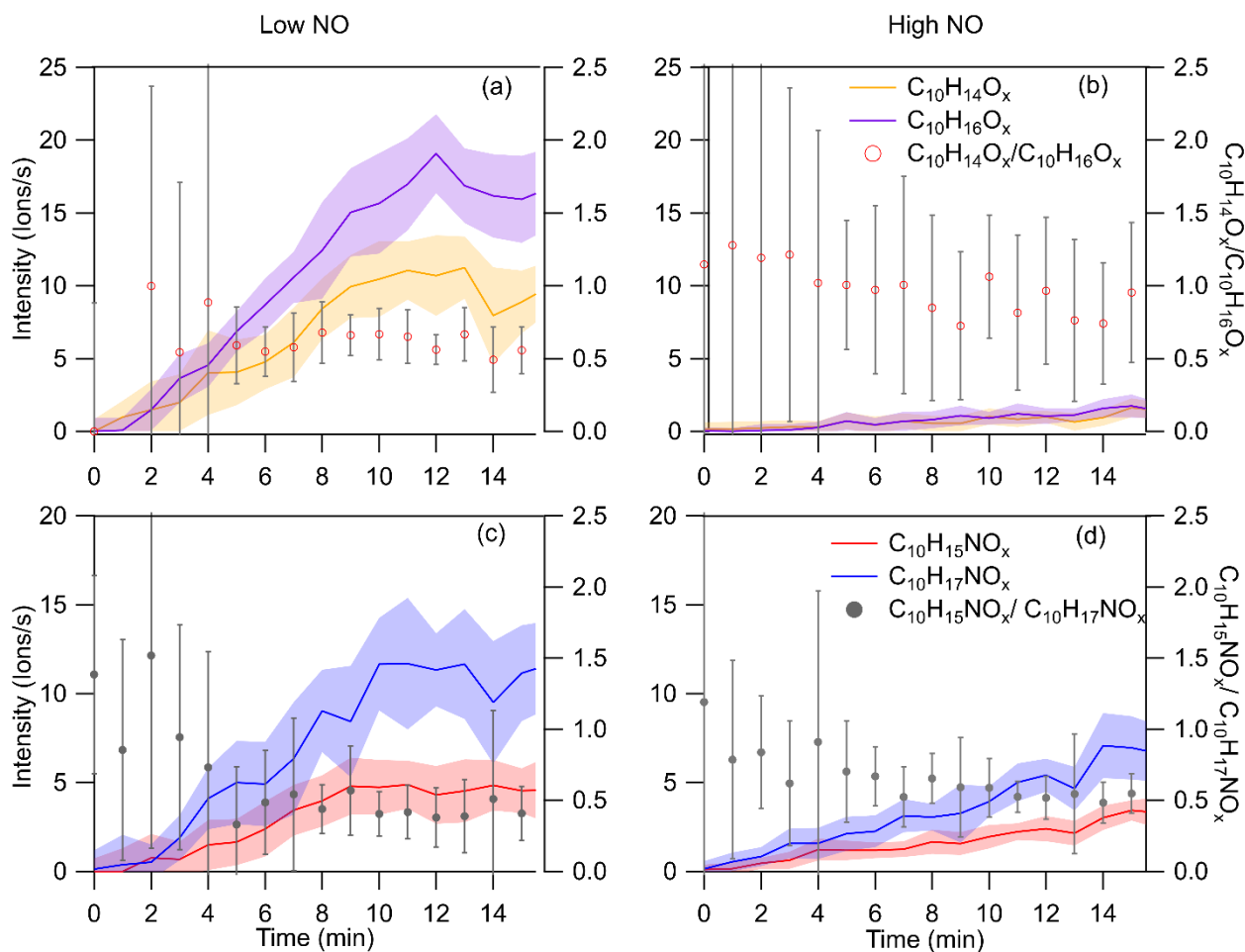


Figure 4. Time series of $C_{10}H_{15}O_x\bullet$ and $C_{10}H_{17}O_x\bullet$ related families of carbonyls and organic nitrates during the first 15 min of the experiments. The carbonyl families $C_{10}H_{14}O_x$ (yellow), $C_{10}H_{16}O_x$ (purple), and their concentration ratio ($C_{10}H_{14}O_x / C_{10}H_{16}O_x$) are shown for (a) low and (b) high NO experiments. Time series for organic nitrate families $C_{10}H_{15}NO_x$ (red) and $C_{10}H_{17}NO_x$ (blue), and concentration ratio of $C_{10}H_{15}NO_x / C_{10}H_{17}NO_x$, are similarly demonstrated in (c) for low NO and (d) high NO experiments. All data are averaged to 1 min and the error bar represents one standard deviation.

3.4 HOM yield

The HOM molar yields during the first 60 min was estimated to be $1.97^{+2.52}_{-1.06}\%$ and $0.29^{+0.38}_{-0.16}\%$ at low and high NO respectively. In brief, the uncertainty (-54%/+128%) was estimated from the HOM signal intensity, VOC concentration, and calibration coefficient of H_2SO_4 as discussed by Zhao et al (2021) (see Supplement S1). It is noted that the HOM yield is not very sensitive to the vapor wall loss rate, since HOM yields only change 11% to -6% upon an 100% increase and 50% decrease in wall loss rate (Zhao et al., 2021). The lower HOM yields at high NO can be partly attributed to lower fractions of dimer products for the inhibitory effect of NO_x as discussed above (Sect. 3.2.3). Within the uncertainty, the HOM yield at high NO in this study is comparable to the HOM yield ($0.93 \pm 0.47\%$) from the photooxidation of limonene in a previous study (Jokinen et al., 2015). The difference in yield at low NO from (Jokinen et al., 2015) may be attributed to different experimental methods and conditions. For example, Jokinen et al. (2015) derived HOM yield from OH oxidation indirectly by comparing the HOM yield in ozonolysis with and without OH scavenger while in this study we determined HOM yield directly for the oxidation of limonene by OH. In ozonolysis, the cross reactions of RO_2 formed from ozonolysis and OH oxidation may produce accretion products thus possibly confounding the results. By directly measuring HOM yield in the oxidation of limonene by OH, such influence is avoided. The NO concentration might be also different between our study and Jokinen et al. (2015). Additionally, the HOM molar yields related to H-abstraction were further determined to be $0.77^{+0.98}_{-0.41}\%$ at low NO and $0.10^{+0.13}_{-0.05}\%$ at high

NO, when assuming that the ratio of all HOM from H-abstraction to those from OH addition is equal to the corresponding ratio for C₁₀-monomers.

4 Conclusions and atmospheric implications

565 In this study, the HOM products in the oxidation of limonene with OH were investigated by using a NO₃⁻-CIMS in the SAPHIR chamber in Jülich. A large number of HOM monomers (C₆₋₁₀) and dimers (C₁₇₋₂₀) were detected and classified according to the number of carbon atoms. Among HOM products, the proportion of HOM monomers is far higher than dimers in both low and high NO condition. C₁₀ HOM were the most abundant monomers at both low and high NO. At low NO, the fraction of organic nitrates (31%) was lower than that of non-nitrate HOM (69%). At high NO, a higher fraction of 41% were observed
570 for organic nitrates. Two major RO₂ radical families, C₁₀H₁₅O_x• and C₁₀H₁₇O_x•, were identified. While C₁₀H₁₇O_x• were formed via OH addition to a double bond, C₁₀H₁₅O_x• is proposed to be formed via H-abstraction by OH on the basis of its molecular formula and the available literature. Although the concentrations of C₁₀H₁₅O_x• related products were less than C₁₀H₁₇O_x• related products, they remained at a comparable magnitude (38.9% vs 55.0% at low NO and 33.7% vs 49.7% at high NO). The formation pathways of C₁₀H₁₅O_x• and C₁₀H₁₇O_x• were proposed on the basis of observed signal intensity, theoretical kinetic
575 calculations, and structure activity relationships (SARs) for autoxidation. At both low and high NO, H-abstraction by OH contributes a significant fraction of HOM (41% and 42% of C₁₀ HOM monomer, respectively), demonstrating that H-abstraction is important to the formation of HOM in the oxidation of limonene with OH radical, and contributes more than expected given the ~34% contribution in the initiation reaction. The key mechanistic difference between OH addition and H-abstraction pathways is that the former does not readily lead to breaking of the six-membered ring without chain termination,
580 whereas H-abstraction leads to fast first-generation autoxidation after an alkoxy-peroxy ring breaking step. C₆-C₉ monomers are proposed to be formed via fragmentation of alkoxy radicals and C₁₇-C₂₀ dimers are proposed to be formed via accretion reactions.

The molar yields of total HOM are estimated to be 1.97^{+2.52%}_{-1.06%} and 0.29^{+0.38%}_{-0.16%} in low and high NO condition. Although the HOM yields in the oxidation of limonene with OH in this study are lower than that in the ozonolysis of limonene (Jokinen et al., 2015), the corresponding SOA mass yields assuming irreversible condensation of HOM can be as high as 4.3% and 0.6%
585 at low NO and high NO, respectively. Similarly, while the gas-phase dimers observed in this study are clearly lower than monomers in abundance, dimers may also be very efficient at condensing onto newly formed particles due to their large size and low volatility. These HOM dimer products are known to have an extremely low volatility due to their size and high degree of oxidation (Tröstl et al., 2016). At 17 ppb NO the RO₂ fate is exclusively reaction with NO, and is representative for all environment where RO₂ loss is dominated by the reaction with NO. Such environment includes urban regions and sub-urban regions, especially in developing countries such as East Asia and South Asia, where our HOM yield can be used to model these areas. In contrast, our HOM yield at low NO is representative for rural and remote continental environment (Rohrer et al., 1998; Lelieveld et al., 2008; Whalley et al., 2011; Moiseenko et al., 2021; Wei et al., 2019). Combined, our results can thus be used directly in atmospheric chemical transport models to simulate the HOM concentrations in many atmospheric regimes (Pye et al., 2019; Xu et al., 2022) and help refine the simulations to assess its importance in new particle formation and particle growth (Zhao et al., 2020).
590
595

This study highlights the importance of the pathway of H-abstraction by OH in competition to OH addition to double bonds in the same molecule at least for HOM formation, which has largely been neglected in current chemical mechanisms. The importance of H-abstraction pathway to HOM formation also in α-pinene+OH oxidation has been shown in our recent study
600 (Shen et al., 2022), and recent experimental work by Williams et al. (2022). H-abstraction in the case of limonene+OH is more prominent than for α-pinene+OH, but the OH abstraction pathway is important in both systems suggesting its importance in other terpenes or even other unsaturated species. We propose that in order to accurately simulate HOM formation from

oxidation of limonene by OH, H-abstraction should be considered in chemical mechanisms of atmospheric models. Considering the key role HOM in SOA particle formation and growth, this study further enables more accurate simulation of chemical composition and concentrations of secondary organic aerosol as well as growth of particles to CCN size in order to assess the impact of SOA on climate.

The experiments in this study were conducted at ambient relevant conditions by using limonene and OH concentrations at ambient levels and using natural sunlight. The major RO₂ loss rate in all experiments is via RO₂+NO. Therefore, the HOM composition and formation pathway can represent a large part of the daytime continental environment. The low NO conditions are representative of forested regions with biogenic monoterpene emissions and influenced by anthropogenic emissions and of rural regions. The experiments at high NO in this study are relevant for the reactions of limonene with OH in urban environment as limonene is also a major component of VCP besides biogenic sources (Nazaroff and Weschler, 2004; Rossignol et al., 2013; Waring, 2016; Gkatzelis et al., 2021).

The fraction of organic nitrate HOM, such as C₁₀H₁₅NO_x and C₁₀H₁₇NO_x, was significant in the total HOM products in both low and high NO conditions examined, highlighting the importance of organic nitrates (ONs). Even at ~0.2 ppb NO, ONs account for a large part (31%) of HOM. ONs are important in the atmosphere as they can serve as an NO_x reservoir (Ng et al., 2017). Highly functionalized ONs have been inferred to be capable of strongly partitioning to the particle phase (Perraud et al., 2012; Ng et al., 2007). The significant amounts of monoterpene-derived ONs that were observed in field campaigns (Massoli et al., 2018; Huang et al., 2019; Lee et al., 2016) indicate that ONs make up a significant fraction of SOA. The abundant presence of ONs highlights the importance of NO_x-driven chemistry in daytime. In most of the continental environment influenced by monoterpene, ONs then likely contribute a large fraction of HOM and SOA, and contribute the organic nitrates and particle formation in the atmosphere.

Acknowledgement

H. Luo, H. Shen, and D. Zhao would like to thank the funding support of National Natural Science Foundation of China (No. 41875145), Science and Technology Commission of Shanghai Municipality (No. 20230711400), and Shanghai International Science and Technology Partnership Project (No. 21230780200). Sungah Kang, Astrid Kiendler-Scharr, and Thomas F. Mentel acknowledge the support by the EU Project FORCeS (grant agreement no. 821205).

Data availability

The supplement provides additional figures and tables, and further information on the CIMS calibration and HOM monomers and dimers with reduced carbon number.

The quantum chemical data (geometries, vibrational wavenumbers, rotational constants, energies, and partition functions) can be found under <https://doi.org/10.26165/JUELICH-DATA/9JVHEK>. [Reviewers: the quantum chemical data can be accessed for reviewing purposes under URL <https://data.fz-juelich.de/privateurl.xhtml?token=60754bd4-d921-449c-9210-7b24839a67ce>]

References

Alecu, I. M., Zheng, J., Zhao, Y., and Truhlar, D. G.: Computational thermochemistry: scale factor databases and scale factors for vibrational frequencies obtained from electronic model chemistries, *J Chem Theory Comput*, 6, 2872-2887, 2010.

- Bartlett, R. J. and Purvis, G. D.: Many-Body Perturbation-Theory, Coupled-Pair Many-Electron Theory, and Importance of
640 Quadruple Excitations for Correlation Problem, *International Journal of Quantum Chemistry*, 14, 561-581, DOI
10.1002/qua.560140504, 1978.
- Berndt, T.: Peroxy Radical Processes and Product Formation in the OH Radical-Initiated Oxidation of α -Pinene for Near-
Atmospheric Conditions, *J Phys Chem A*, 125, 9151-9160, 10.1021/acs.jpca.1c05576, 2021.
- Berndt, T., Mentler, B., Scholz, W., Fischer, L., Herrmann, H., Kulmala, M., and Hansel, A.: Accretion Product Formation
645 from Ozonolysis and OH Radical Reaction of α -Pinene: Mechanistic Insight and the Influence of Isoprene and Ethylene,
Environ Sci Technol, 52, 11069-11077, 10.1021/acs.est.8b02210, 2018a.
- Berndt, T., Scholz, W., Mentler, B., Fischer, L., Herrmann, H., Kulmala, M., and Hansel, A.: Accretion Product Formation
from Self- and Cross-Reactions of RO₂ Radicals in the Atmosphere, *Angew Chem Int Ed Engl*, 57, 3820-3824,
10.1002/anie.201710989, 2018b.
- 650 Berndt, T., Richters, S., Jokinen, T., Hyttinen, N., Kurtén, T., Otkjær, R. V., Kjaergaard, H. G., Stratmann, F., Herrmann, H.,
Sipilä, M., Kulmala, M., and Ehn, M.: Hydroxyl radical-induced formation of highly oxidized organic compounds, *Nat
Commun*, 7, 13677, 10.1038/ncomms13677, 2016.
- Bianchi, F., Kurtén, T., Riva, M., Mohr, C., Rissanen, M. P., Roldin, P., Berndt, T., Crouse, J. D., Wennberg, P. O., Mentel,
T. F., Wildt, J., Junninen, H., Jokinen, T., Kulmala, M., Worsnop, D. R., Thornton, J. A., Donahue, N., Kjaergaard, H. G.,
655 and Ehn, M.: Highly Oxygenated Organic Molecules (HOM) from Gas-Phase Autoxidation Involving Peroxy Radicals: A
Key Contributor to Atmospheric Aerosol, *Chem Rev*, 119, 3472-3509, 10.1021/acs.chemrev.8b00395, 2019.
- Braure, T., Bedjanian, Y., Romanias, M. N., Morin, J., Riffault, V., Tomas, A., and Coddeville, P.: Experimental study of the
reactions of limonene with OH and OD radicals: kinetics and products, *J Phys Chem A*, 118, 9482-9490, 10.1021/jp507180g,
2014.
- 660 Chen, X. and Hopke, P. K.: A chamber study of secondary organic aerosol formation by limonene ozonolysis, *Indoor Air*, 20,
320-328, 10.1111/j.1600-0668.2010.00656.x, 2010.
- Crouse, J. D., Nielsen, L. B., Jørgensen, S., Kjaergaard, H. G., and Wennberg, P. O.: Autoxidation of Organic Compounds
in the Atmosphere, *J Phys Chem Lett*, 4, 3513-3520, 10.1021/jz4019207, 2013.
- Dash, M. R. and Rajakumar, B.: Theoretical investigations of the gas phase reaction of limonene (C₁₀H₁₆) with OH radical,
665 *Mol Phys*, 113, 3202-3215, 10.1080/00268976.2015.1014002, 2015.
- Dunning, T. H.: Gaussian basis sets for use in correlated molecular calculations. I. The atoms boron through neon and hydrogen,
J Chem Phys, 90, 1007-1023, 10.1063/1.456153, 1989.
- Dunning, T. H., Peterson, K. A., and Wilson, A. K.: Gaussian basis sets for use in correlated molecular calculations. X. The
atoms aluminum through argon revisited, *The Journal of Chemical Physics*, 114, 9244-9253, 10.1063/1.1367373, 2001.
- 670 Eckart, C.: The Penetration of a Potential Barrier by Electrons, *Phys Rev*, 35, 1303-1309, 10.1103/PhysRev.35.1303, 1930.
- Eddingsaas, N. C., Loza, C. L., Yee, L. D., Seinfeld, J. H., and Wennberg, P. O.: α -pinene photooxidation under controlled
chemical conditions – Part I: Gas-phase composition in low- and high-NO_x environments, *Atmos Chem Phys*, 12, 6489-
6504, 10.5194/acp-12-6489-2012, 2012.
- Ehn, M., Berndt, T., Wildt, J., and Mentel, T.: Highly Oxygenated Molecules from Atmospheric Autoxidation of Hydrocarbons:
675 A Prominent Challenge for Chemical Kinetics Studies, *Int J Chem Kinet*, 49, 821-831, 10.1002/kin.21130, 2017.
- Ehn, M., Kleist, E., Junninen, H., Petäjä, T., Lönn, G., Schobesberger, S., Dal Maso, M., Trimborn, A., Kulmala, M., Worsnop,
D. R., Wahner, A., Wildt, J., and Mentel, T. F.: Gas phase formation of extremely oxidized pinene reaction products in
chamber and ambient air, *Atmos Chem Phys*, 12, 5113-5127, 10.5194/acp-12-5113-2012, 2012.
- Ehn, M., Thornton, J. A., Kleist, E., Sipilä, M., Junninen, H., Pullinen, I., Springer, M., Rubach, F., Tillmann, R., Lee, B.,
680 Lopez-Hilfiker, F., Andres, S., Acir, I. H., Rissanen, M., Jokinen, T., Schobesberger, S., Kangasluoma, J., Kontkanen, J.,
Nieminen, T., Kurtén, T., Nielsen, L. B., Jørgensen, S., Kjaergaard, H. G., Canagaratna, M., Maso, M. D., Berndt, T., Petäjä,

- T., Wahner, A., Kerminen, V. M., Kulmala, M., Worsnop, D. R., Wildt, J., and Mentel, T. F.: A large source of low-volatility secondary organic aerosol, *Nature*, 506, 476-479, 10.1038/nature13032, 2014.
- 685 Finlayson-Pitts, B. J. and Pitts, J. N. J.: *Chemistry of the Upper and Lower Atmosphere: Theory, Experiments, and Applications*, Academic Press, San Diego, San Francisco, New York, Boston London, Sydney Tokyo2000.
- Friedman, B. and Farmer, D. K.: SOA and gas phase organic acid yields from the sequential photooxidation of seven monoterpenes, *Atmos Environ*, 187, 335-345, 10.1016/j.atmosenv.2018.06.003, 2018.
- 690 Frisch, M. J., Trucks, G. W., Schlegel, H. B., and G. E. Scuseria, M. A. R., J. R. Cheeseman, G. Scalmani, V. Barone, G. A. Petersson, H. Nakatsuji, X. Li, M. Caricato, A. V. Marenich, J. Bloino, B. G. Janesko, R. Gomperts, B. Mennucci, H. P. Hratchian, J. V. Ortiz, A. F. Izmaylov, J. L. Sonnenberg, Williams, F. Ding, F. Lipparini, F. Egidi, J. Goings, B. Peng, A. Petrone, T. Henderson, D. Ranasinghe, V. G. Zakrzewski, J. Gao, N. Rega, G. Zheng, W. Liang, M. Hada, M. Ehara, K. Toyota, R. Fukuda, J. Hasegawa, M. Ishida, T. Nakajima, Y. Honda, O. Kitao, H. Nakai, T. Vreven, K. Throssell, J. A. Montgomery Jr., J. E. Peralta, F. Ogliaro, M. J. Bearpark, J. J. Heyd, E. N. Brothers, K. N. Kudin, V. N. Staroverov, T. A. Keith, R. Kobayashi, J. Normand, K. Raghavachari, A. P. Rendell, J. C. Burant, S. S. Iyengar, J. Tomasi, M. Cossi, J. M. 695 Millam, M. Klene, C. Adamo, R. Cammi, J. W. Ochterski, R. L. Martin, K. Morokuma, O. Farkas, J. B. Foresman, D. J. Fox.: *Gaussian 09 Revision E.01*, Gaussian Inc., [code], 2016.
- Fuchs, H., Bohn, B., Hofzumahaus, A., Holland, F., Lu, K. D., Nehr, S., Rohrer, F., and Wahner, A.: Detection of HO₂ by laser-induced fluorescence: calibration and interferences from RO₂ radicals, *Atmos. Meas. Tech.*, 4, 1209-1225, 10.5194/amt-4-1209-2011, 2011.
- 700 Fuchs, H., Dorn, H.-P., Bachner, M., Bohn, B., Brauers, T., Gomm, S., Hofzumahaus, A., Holland, F., Nehr, S., Rohrer, F., Tillmann, R., and Wahner, A.: Comparison of OH concentration measurements by DOAS and LIF during SAPHIR chamber experiments at high OH reactivity and low NO concentration, *Atmos Meas Tech*, 5, 1611-1626, 10.5194/amt-5-1611-2012, 2012.
- Gkatzelis, G. I., Coggon, M. M., McDonald, B. C., Peischl, J., Gilman, J. B., Aikin, K. C., Robinson, M. A., Canonaco, F., 705 Prevot, A. S. H., Trainer, M., and Warneke, C.: Observations Confirm that Volatile Chemical Products Are a Major Source of Petrochemical Emissions in U.S. Cities, *Environ Sci Technol*, 55, 4332-4343, 10.1021/acs.est.0c05471, 2021.
- Goerigk, L., Hansen, A., Bauer, C., Ehrlich, S., Najibi, A., and Grimme, S.: A look at the density functional theory zoo with the advanced GMTKN55 database for general main group thermochemistry, kinetics and noncovalent interactions, *Phys Chem Chem Phys*, 19, 32184-32215, 10.1039/c7cp04913g, 2017.
- 710 Gong, Y., Chen, Z., and Li, H.: The oxidation regime and SOA composition in limonene ozonolysis: roles of different double bonds, radicals, and water, *Atmos Chem Phys*, 18, 15105-15123, 10.5194/acp-18-15105-2018, 2018.
- Griffin, R. J., Cocker, D. R., Flagan, R. C., and Seinfeld, J. H.: Organic aerosol formation from the oxidation of biogenic hydrocarbons, *J Geophys Res*, 104, 3555-3567, 10.1029/1998jd100049, 1999.
- Grimme, S., Ehrlich, S., and Goerigk, L.: Effect of the damping function in dispersion corrected density functional theory, *J 715 Comput Chem*, 32, 1456-1465, 10.1002/jcc.21759, 2011.
- Guenther, A. B., Jiang, X., Heald, C. L., Sakulyanontvittaya, T., Duhl, T., Emmons, L. K., and Wang, X.: The Model of Emissions of Gases and Aerosols from Nature version 2.1 (MEGAN2.1): an extended and updated framework for modeling biogenic emissions, *Geosci Model Dev*, 5, 1471-1492, 10.5194/gmd-5-1471-2012, 2012.
- Guo, Y., Shen, H., Pullinen, I., Luo, H., Kang, S., Vereecken, L., Fuchs, H., Hallquist, M., Acir, I.-H., Tillmann, R., Rohrer, 720 F., Wildt, J., Kiendler-Scharr, A., Wahner, A., Zhao, D., and Mentel, T. F.: Identification of highly oxygenated organic molecules and their role in aerosol formation in the reaction of limonene with nitrate radical, *Atmos Chem Phys*, 22, 11323-11346, 10.5194/acp-2022-85, 2022.
- Hakola, H., Arey, J., Aschmann, S. M., and Atkinson, R.: Product Formation from the Gas-Phase Reactions of OH Radicals and O₃ with a Series of Monoterpenes, *J Atmos Chem*, 18, 75-102, Doi 10.1007/Bf00694375, 1994.

- 725 Hallquist, M., Wenger, J. C., Baltensperger, U., Rudich, Y., Simpson, D., Claeys, M., Dommen, J., Donahue, N. M., George, C., Goldstein, A. H., Hamilton, J. F., Herrmann, H., Hoffmann, T., Iinuma, Y., Jang, M., Jenkin, M. E., Jimenez, J. L., Kiendler-Scharr, A., Maenhaut, W., McFiggans, G., Mentel, T. F., Monod, A., Prévôt, A. S. H., Seinfeld, J. H., Surratt, J. D., Szmigielski, R., and Wildt, J.: The formation, properties and impact of secondary organic aerosol: current and emerging issues, *Atmos Chem Phys*, 9, 5155-5236, 2009.
- 730 Hammes, J., Lutz, A., Mentel, T., Faxon, C., and Hallquist, M.: Carboxylic acids from limonene oxidation by ozone and hydroxyl radicals: insights into mechanisms derived using a FIGAERO-CIMS, *Atmos Chem Phys*, 19, 13037-13052, 10.5194/acp-19-13037-2019, 2019.
- Huang, W., Saathoff, H., Shen, X., Ramisetty, R., Leisner, T., and Mohr, C.: Chemical Characterization of Highly Functionalized Organonitrates Contributing to Night-Time Organic Aerosol Mass Loadings and Particle Growth, *Environ Sci Technol*, 53, 1165-1174, 10.1021/acs.est.8b05826, 2019.
- 735 Hyttinen, N., Rissanen, M. P., and Kurtén, T.: Computational Comparison of Acetate and Nitrate Chemical Ionization of Highly Oxidized Cyclohexene Ozonolysis Intermediates and Products, *The Journal of Physical Chemistry A*, 121, 2172-2179, 10.1021/acs.jpca.6b12654, 2017.
- Hyttinen, N., Kupiainen-Määttä, O., Rissanen, M. P., Muuronen, M., Ehn, M., and Kurtén, T.: Modeling the Charging of Highly Oxidized Cyclohexene Ozonolysis Products Using Nitrate-Based Chemical Ionization, *The Journal of Physical Chemistry A*, 119, 6339-6345, 10.1021/acs.jpca.5b01818, 2015.
- 740 Jaoui, M., Corse, E., Kleindienst, T. E., Offenberg, J. H., Lewandowski, M., and Edney, E. O.: Analysis of Secondary Organic Aerosol Compounds from the Photooxidation of d Limonene in the Presence of NO_x and their Detection in Ambient PM_{2.5}, *Environ Sci Technol*, 40, 3819-3828, 2006.
- 745 Jenkin, M. E., Saunders, S. M., and Pilling, M. J.: The tropospheric degradation of volatile organic compounds: a protocol for mechanism development, *Atmos Environ*, 31, 81-104, 1997.
- Jenkin, M. E., Valorso, R., Aumont, B., and Rickard, A. R.: Estimation of rate coefficients and branching ratios for reactions of organic peroxy radicals for use in automated mechanism construction, *Atmos Chem Phys*, 19, 7691-7717, 10.5194/acp-19-7691-2019, 2019.
- 750 Jenkin, M. E., Valorso, R., Aumont, B., Rickard, A. R., and Wallington, T. J.: Estimation of rate coefficients and branching ratios for gas-phase reactions of OH with aliphatic organic compounds for use in automated mechanism construction, *Atmos Chem Phys*, 18, 9297-9328, 10.5194/acp-18-9297-2018, 2018.
- Johnston, H. S. and Heicklen, J.: Tunnelling Corrections for Unsymmetrical Eckart Potential Energy Barriers, *J Phys Chem*, 66, 532-533, 1962.
- 755 Jokinen, T., Sipilä, M., Richters, S., Kerminen, V. M., Paasonen, P., Stratmann, F., Worsnop, D., Kulmala, M., Ehn, M., Herrmann, H., and Berndt, T.: Rapid autoxidation forms highly oxidized RO₂ radicals in the atmosphere, *Angew Chem Int Ed*, 53, 14596-14600, 10.1002/anie.201408566, 2014.
- Jokinen, T., Berndt, T., Makkonen, R., Kerminen, V. M., Junninen, H., Paasonen, P., Stratmann, F., Herrmann, H., Guenther, A. B., Worsnop, D. R., Kulmala, M., Ehn, M., and Sipilä, M.: Production of extremely low volatile organic compounds from biogenic emissions: Measured yields and atmospheric implications, *Proc Natl Acad Sci U S A*, 112, 7123-7128, 10.1073/pnas.1423977112, 2015.
- 760 Jørgensen, S., Knap, H. C., Otkjær, R. V., Jensen, A. M., Kjeldsen, M. L., Wennberg, P. O., and Kjaergaard, H. G.: Rapid Hydrogen Shift Scrambling in Hydroperoxy-Substituted Organic Peroxy Radicals, *J Phys Chem A*, 120, 266-275, 10.1021/acs.jpca.5b06768, 2016.
- 765 Kanakidou, M., Seinfeld, J. H., Pandis, S. N., Barnes, I., Dentener, F. J., Facchini, M. C., Van Dingenen, R., Ervens, B., Nenes, A., Nielsen, C. J., Swietlicki, E., Putaud, J. P., Balkanski, Y., Fuzzi, S., Horth, J., Moortgat, G. K., Winterhalter, R., Myhre,

- C. E. L., Tsigaridis, K., Vignati, E., Stephanou, E. G., and Wilson, J.: Organic aerosol and global climate modelling: A review, *Atmos Chem Phys*, 5, 1053-1123, 2005.
- 770 Kenseth, C. M., Huang, Y., Zhao, R., Dalleska, N. F., Hethcox, J. C., Stoltz, B. M., and Seinfeld, J. H.: Synergistic O₃ + OH oxidation pathway to extremely low-volatility dimers revealed in beta-pinene secondary organic aerosol, *Proc Natl Acad Sci U S A*, 115, 8301-8306, 10.1073/pnas.1804671115, 2018.
- Kirkby, J., Duplissy, J., Sengupta, K., Frege, C., Gordon, H., Williamson, C., Heinritzi, M., Simon, M., Yan, C., Almeida, J., Tröstl, J., Nieminen, T., Ortega, I. K., Wagner, R., Adamov, A., Amorim, A., Bernhammer, A. K., Bianchi, F., Breitenlechner, M., Brilke, S., Chen, X., Craven, J., Dias, A., Ehrhart, S., Flagan, R. C., Franchin, A., Fuchs, C., Guida, R., 775 Hakala, J., Hoyle, C. R., Jokinen, T., Junninen, H., Kangasluoma, J., Kim, J., Krapf, M., Kürten, A., Laaksonen, A., Lehtipalo, K., Makhmutov, V., Mathot, S., Molteni, U., Onnela, A., Peräkylä, O., Piel, F., Petäjä, T., Praplan, A. P., Pringle, K., Rap, A., Richards, N. A., Riipinen, I., Rissanen, M. P., Rondo, L., Sarnela, N., Schobesberger, S., Scott, C. E., Seinfeld, J. H., Sipilä, M., Steiner, G., Stozhkov, Y., Stratmann, F., Tomé, A., Virtanen, A., Vogel, A. L., Wagner, A. C., Wagner, P. E., Weingartner, E., Wimmer, D., Winkler, P. M., Ye, P., Zhang, X., Hansel, A., Dommen, J., Donahue, N. M., Worsnop, 780 D. R., Baltensperger, U., Kulmala, M., Carslaw, K. S., and Curtius, J.: Ion-induced nucleation of pure biogenic particles, *Nature*, 533, 521-526, 10.1038/nature17953, 2016.
- Knap, H. C. and Jørgensen, S.: Rapid Hydrogen Shift Reactions in Acyl Peroxy Radicals, *J Phys Chem A*, 121, 1470-1479, 10.1021/acs.jpca.6b12787, 2017.
- Koch, S., Winterhalter, R., Uherek, E., Koloff, A., Neeb, P., and Moortgat, G. K.: Formation of new particles in the gas-phase 785 ozonolysis of monoterpenes, *Atmos Environ*, 34, 4031-4042, 2000.
- Krechmer, J. E., Coggon, M. M., Massoli, P., Nguyen, T. B., Crounse, J. D., Hu, W., Day, D. A., Tyndall, G. S., Henze, D. K., Rivera-Rios, J. C., Nowak, J. B., Kimmel, J. R., Mauldin, R. L., III, Stark, H., Jayne, J. T., Sipilä, M., Junninen, H., Clair, J. M. S., Zhang, X., Feiner, P. A., Zhang, L., Miller, D. O., Brune, W. H., Keutsch, F. N., Wennberg, P. O., Seinfeld, J. H., Worsnop, D. R., Jimenez, J. L., and Canagaratna, M. R.: Formation of Low Volatility Organic Compounds and Secondary 790 Organic Aerosol from Isoprene Hydroxyhydroperoxide Low-NO Oxidation, *Environ Sci Technol*, 49, 10330-10339, 10.1021/acs.est.5b02031, 2015.
- Larsen, B. R., Di Bella, D., Glasius, M., Winterhalter, R., Jensen, N. R., and Hjorth, J.: Gas-phase OH oxidation of monoterpenes: Gaseous and particulate products, *J. Atmos. Chem.*, 38, 231-276, Doi 10.1023/A:1006487530903, 2001.
- Lee, A., Goldstein, A. H., Kroll, J. H., Ng, N. L., Varutbangkul, V., Flagan, R. C., and Seinfeld, J. H.: Gas-phase products and 795 secondary aerosol yields from the photooxidation of 16 different terpenes, *J Geophys Res*, 111, 10.1029/2006jd007050, 2006a.
- Lee, A., Goldstein, A. H., Keywood, M. D., Gao, S., Varutbangkul, V., Bahreini, R., Ng, N. L., Flagan, R. C., and Seinfeld, J. H.: Gas-phase products and secondary aerosol yields from the ozonolysis of ten different terpenes, *J Geophys Res*, 111, 10.1029/2005jd006437, 2006b.
- 800 Lee, B. H., Mohr, C., Lopez-Hilfiker, F. D., Lutz, A., Hallquist, M., Lee, L., Romer, P., Cohen, R. C., Iyer, S., Kurtén, T., Hu, W., Day, D. A., Campuzano-Jost, P., Jimenez, J. L., Xu, L., Ng, N. L., Guo, H., Weber, R. J., Wild, R. J., Brown, S. S., Koss, A., de Gouw, J., Olson, K., Goldstein, A. H., Seco, R., Kim, S., McAvey, K., Shepson, P. B., Starn, T., Baumann, K., Edgerton, E. S., Liu, J., Shilling, J. E., Miller, D. O., Brune, W., Schobesberger, S., D'Ambro, E. L., and Thornton, J. A.: Highly functionalized organic nitrates in the southeast United States: Contribution to secondary organic aerosol and reactive 805 nitrogen budgets, *Proc Natl Acad Sci U S A*, 113, 1516-1521, 10.1073/pnas.1508108113, 2016.
- Lelieveld, J., Butler, T. M., Crowley, J. N., Dillon, T. J., Fischer, H., Ganzeveld, L., Harder, H., Lawrence, M. G., Martinez, M., Taraborrelli, D., and Williams, J.: Atmospheric oxidation capacity sustained by a tropical forest, *Nature*, 452, 737-740, 10.1038/nature06870, 2008.

- Massoli, P., Stark, H., Canagaratna, M. R., Krechmer, J. E., Xu, L., Ng, N. L., Mauldin, III., Roy L., Yan, C., Kimmel, J.,
810 Misztal, P. K., Jimenez, J. L., Jayne, J. T., and Worsnop, D. R.: Ambient Measurements of Highly Oxidized Gas-Phase
Molecules during the Southern Oxidant and Aerosol Study (SOAS) 2013, *ACS Earth Space Chem*, 2, 653-672,
10.1021/acsearthspacechem.8b00028, 2018.
- Mayorga, R., Xia, Y., Zhao, Z., Long, B., and Zhang, H.: Peroxy Radical Autoxidation and Sequential Oxidation in Organic
Nitrate Formation during Limonene Nighttime Oxidation, *Environ Sci Technol*, 56, 15337-15346, 10.1021/acs.est.2c04030,
815 2022.
- McFiggans, G., Mentel, T. F., Wildt, J., Pullinen, I., Kang, S., Kleist, E., Schmitt, S., Springer, M., Tillmann, R., Wu, C., Zhao,
D., Hallquist, M., Faxon, C., Le Breton, M., Hallquist, Å. M., Simpson, D., Bergström, R., Jenkin, M. E., Ehn, M., Thornton,
J. A., Alfarra, M. R., Bannan, T. J., Percival, C. J., Priestley, M., Topping, D., and Kiendler-Scharr, A.: Secondary organic
aerosol reduced by mixture of atmospheric vapours, *Nature*, 565, 587-593, 10.1038/s41586-018-0871-y, 2019.
- 820 Mentel, T. F., Springer, M., Ehn, M., Kleist, E., Pullinen, I., Kurtén, T., Rissanen, M., Wahner, A., and Wildt, J.: Formation
of highly oxidized multifunctional compounds: autoxidation of peroxy radicals formed in the ozonolysis of alkenes –
deduced from structure–product relationships, *Atmos Chem Phys*, 15, 6745-6765, 10.5194/acp-15-6745-2015, 2015.
- Miller, J. A., Pilling, M. J., and Troe, J.: Unravelling combustion mechanisms through a quantitative understanding of
elementary reactions, *P Combust Inst*, 30, 43-88, 10.1016/j.proci.2004.08.281, 2005.
- 825 Moiseenko, K. B., Vasileva, A. V., Skorokhod, A. I., Belikov, I. B., Repin, A. Y., and Shtabkin, Y. A.: Regional Impact of
Ozone Precursor Emissions on NO_x and O₃ Levels at ZOTTO Tall Tower in Central Siberia, *Earth Space Sci.*, 8,
10.1029/2021ea001762, 2021.
- Møller, K. H., Bates, K. H., and Kjaergaard, H. G.: The Importance of Peroxy Radical Hydrogen-Shift Reactions in
Atmospheric Isoprene Oxidation, *J Phys Chem A*, 123, 920-932, 10.1021/acs.jpca.8b10432, 2019.
- 830 Molteni, U., Simon, M., Heinritzi, M., Hoyle, C. R., Bernhammer, A.-K., Bianchi, F., Breitenlechner, M., Brilke, S., Dias, A.,
Duplissy, J., Frege, C., Gordon, H., Heyn, C., Jokinen, T., Kürten, A., Lehtipalo, K., Makhmutov, V., Petäjä, T., Pieber, S.
M., Praplan, A. P., Schobesberger, S., Steiner, G., Stozhkov, Y., Tomé, A., Tröstl, J., Wagner, A. C., Wagner, R., Williamson,
C., Yan, C., Baltensperger, U., Curtius, J., Donahue, N. M., Hansel, A., Kirkby, J., Kulmala, M., Worsnop, D. R., and
Dommen, J.: Formation of Highly Oxygenated Organic Molecules from α -Pinene Ozonolysis: Chemical Characteristics,
835 Mechanism, and Kinetic Model Development, *ACS Earth Space Chem*, 3, 873-883, 10.1021/acsearthspacechem.9b00035,
2019.
- Nazaroff, W. W. and Weschler, C. J.: Cleaning products and air fresheners: exposure to primary and secondary air pollutants,
Atmos Environ, 38, 2841-2865, 10.1016/j.atmosenv.2004.02.040, 2004.
- Ng, N. L., Chhabra, P. S., Chan, A. W. H., Surratt, J. D., Kroll, J. H., Kwan, A. J., McCabe, D. C., Wennberg, P. O., Sorooshian,
840 A., Murphy, S. M., Dalleska, N. F., Flagan, R. C., and Seinfeld, J. H.: Effect of NO_x level on secondary organic aerosol
(SOA) formation from the photooxidation of terpenes, *Atmos Chem Phys*, 7, 5159-5174, 2007.
- Ng, N. L., Brown, S. S., Archibald, A. T., Atlas, E., Cohen, R. C., Crowley, J. N., Day, D. A., Donahue, N. M., Fry, J. L.,
Fuchs, H., Griffin, R. J., Guzman, M. I., Herrmann, H., Hodzic, A., Iinuma, Y., Jimenez, J. L., Kiendler-Scharr, A., Lee, B.
H., Luecken, D. J., Mao, J., McLaren, R., Mutzel, A., Osthoff, H. D., Ouyang, B., Picquet-Varrault, B., Platt, U., Pye, H. O.
845 T., Rudich, Y., Schwantes, R. H., Shiraiwa, M., Stutz, J., Thornton, J. A., Tilgner, A., Williams, B. J., and Zaveri, R. A.:
Nitrate radicals and biogenic volatile organic compounds: oxidation, mechanisms, and organic aerosol, *Atmos Chem Phys*,
17, 2103-2162, 10.5194/acp-17-2103-2017, 2017.
- Novelli, A., Cho, C., Fuchs, H., Hofzumahaus, A., Rohrer, F., Tillmann, R., Kiendler-Scharr, A., Wahner, A., and Vereecken,
L.: Experimental and theoretical study on the impact of a nitrate group on the chemistry of alkoxy radicals, *Phys Chem*
850 *Chem Phys*, 23, 5474-5495, 10.1039/d0cp05555g, 2021.

- Nozière, B. and Vereecken, L.: Direct Observation of Aliphatic Peroxy Radical Autoxidation and Water Effects: An Experimental and Theoretical Study, *Angew Chem Int Ed*, 58, 13976-13982, 10.1002/anie.201907981, 2019.
- Pang, J. Y. S., Novelli, A., Kaminski, M., Acir, I.-H., Bohn, B., Carlsson, P. T. M., Cho, C., Dorn, H.-P., Hofzumahaus, A., Li, X., Lutz, A., Nehr, S., Reimer, D., Rohrer, F., Tillmann, R., Wegener, R., Kiendler-Scharr, A., Wahner, A., and Fuchs, H.: Investigation of the limonene photooxidation by OH at different NO concentrations in the atmospheric simulation chamber SAPHIR, *Atmos Chem Phys Discuss*, 10.5194/acp-2022-239, 2022.
- Peeters, J., Vandenberk, S., Piessens, E., and Pultau, V.: H-atom abstraction in reactions of cyclic polyalkenes with OH, *Chemosphere*, 38, 1189-1195, 1999.
- Perraud, V., Bruns, E. A., Ezell, M. J., Johnson, S. N., Yu, Y., Alexander, M. L., Zelenyuk, A., Imre, D., Chang, W. L., Dabdub, D., Pankow, J. F., and Finlayson-Pitts, B. J.: Nonequilibrium atmospheric secondary organic aerosol formation and growth, *Proc Natl Acad Sci U S A*, 109, 2836-2841, 10.1073/pnas.1119909109, 2012.
- Piletic, I. R. and Kleindienst, T. E.: Rates and Yields of Unimolecular Reactions Producing Highly Oxidized Peroxy Radicals in the OH-Induced Autoxidation of α -Pinene, β -Pinene, and Limonene, *J Phys Chem A*, 126, 88-100, 10.1021/acs.jpca.1c07961, 2022.
- Praske, E., Otkjær, R. V., Crouse, J. D., Hethcox, J. C., Stoltz, B. M., Kjaergaard, H. G., and Wennberg, P. O.: Intramolecular Hydrogen Shift Chemistry of Hydroperoxy-Substituted Peroxy Radicals, *J Phys Chem A*, 123, 590-600, 10.1021/acs.jpca.8b09745, 2019.
- Pullinen, I., Schmitt, S., Kang, S., Sarrafzadeh, M., Schlag, P., Andres, S., Kleist, E., Mentel, T. F., Rohrer, F., Springer, M., Tillmann, R., Wildt, J., Wu, C., Zhao, D., Wahner, A., and Kiendler-Scharr, A.: Impact of NO_x on secondary organic aerosol (SOA) formation from α -pinene and β -pinene photooxidation: the role of highly oxygenated organic nitrates, *Atmos Chem Phys*, 20, 10125-10147, 10.5194/acp-20-10125-2020, 2020.
- Pye, H. O. T., D'Ambro, E. L., Lee, B., Schobesberger, S., Takeuchi, M., Zhao, Y., Lopez-Hilfiker, F., Liu, J. M., Shilling, J. E., Xing, J., Mathur, R., Middlebrook, A. M., Liao, J., Welti, A., Graus, M., Warneke, C., de Gouw, J. A., Holloway, J. S., Ryerson, T. B., Pollack, I. B., and Thornton, J. A.: Anthropogenic enhancements to production of highly oxygenated molecules from autoxidation, *Proc. Nat. Acad. Sci. U.S.A.*, 116, 6641-6646, 10.1073/pnas.1810774116, 2019.
- Quéléver, L. L. J., Kristensen, K., Normann Jensen, L., Rosati, B., Teiwes, R., Daellenbach, K. R., Peräkylä, O., Roldin, P., Bossi, R., Pedersen, H. B., Glasius, M., Bilde, M., and Ehn, M.: Effect of temperature on the formation of highly oxygenated organic molecules (HOMs) from alpha-pinene ozonolysis, *Atmos Chem Phys*, 19, 7609-7625, 10.5194/acp-19-7609-2019, 2019.
- Rio, C., Flaud, P. M., Loison, J. C., and Villenave, E.: Experimental revaluation of the importance of the abstraction channel in the reactions of monoterpenes with OH radicals, *ChemPhysChem*, 11, 3962-3970, 10.1002/cphc.201000518, 2010.
- Rissanen, M. P., Kurtén, T., Sipilä, M., Thornton, J. A., Kangasluoma, J., Sarnela, N., Junninen, H., Jørgensen, S., Schallhart, S., Kajos, M. K., Taipale, R., Springer, M., Mentel, T. F., Ruuskanen, T., Petäjä, T., Worsnop, D. R., Kjaergaard, H. G., and Ehn, M.: The formation of highly oxidized multifunctional products in the ozonolysis of cyclohexene, *J Am Chem Soc*, 136, 15596-15606, 10.1021/ja507146s, 2014.
- Rohrer, F., Bohn, B., Brauers, T., Brüning, D., Johnen, F. J., Wahner, A., and Kleffmann, J.: Characterisation of the photolytic HONO-source in the atmosphere simulation chamber SAPHIR, *Atmos Chem Phys*, 5, 2189-2201, 2005.
- Rohrer, F., Brüning, D., Grobler, E. S., Weber, M., Ehhalt, D. H., Neubert, R., Schussler, W., and Levin, I.: Mixing ratios and photostationary state of NO and NO₂ observed during the POPCORN field campaign at a rural site in Germany, *J. Atmos. Chem.*, 31, 119-137, Doi 10.1023/A:1006166116242, 1998.
- Romonosky, D. E., Laskin, A., Laskin, J., and Nizkorodov, S. A.: High-resolution mass spectrometry and molecular characterization of aqueous photochemistry products of common types of secondary organic aerosols, *J Phys Chem A*, 119, 2594-2606, 10.1021/jp509476r, 2015.

- Rossignol, S., Rio, C., Ustache, A., Fable, S., Nicolle, J., Môme, A., D'Anna, B., Nicolas, M., Leoz, E., and Chiappini, L.: The use of a housecleaning product in an indoor environment leading to oxygenated polar compounds and SOA formation: Gas and particulate phase chemical characterization, *Atmos Environ*, 75, 196-205, 10.1016/j.atmosenv.2013.03.045, 2013.
- Saathoff, H., Naumann, K.-H., Möhler, O., Jonsson, Å. M., Hallquist, M., Kiendler-Scharr, A., Mentel, T. F., Tillmann, R., and Schurath, U.: A chamber study of secondary organic aerosol formation by limonene ozonolysis, *Atmos Chem Phys*, 9, 1551-1577, 2009.
- Shen, H., Vereecken, L., Kang, S., Pullinen, I., Fuchs, H., Zhao, D., and Mentel, T. F.: Unexpected significance of a minor reaction pathway in daytime formation of biogenic highly oxygenated organic compounds, *Sci Adv*, 8, 1-11, 2022.
- Shen, H., Zhao, D., Pullinen, I., Kang, S., Vereecken, L., Fuchs, H., Acir, I. H., Tillmann, R., Rohrer, F., Wildt, J., Kiendler-Scharr, A., Wahner, A., and Mentel, T. F.: Highly Oxygenated Organic Nitrates Formed from NO₃ Radical-Initiated Oxidation of β-Pinene, *Environ Sci Technol*, 55, 15658-15671, 10.1021/acs.est.1c03978, 2021.
- Taatjes, C. A.: Uncovering the Fundamental Chemistry of Alkyl+O₂ Reactions via Measurements of Product Formation, *J Phys Chem A*, 110, 4299-4312, 2006.
- Tomaz, S., Wang, D., Zabalegui, N., Li, D., Lamkaddam, H., Bachmeier, F., Vogel, A., Monge, M. E., Perrier, S., Baltensperger, U., George, C., Rissanen, M., Ehn, M., El Haddad, I., and Riva, M.: Structures and reactivity of peroxy radicals and dimeric products revealed by online tandem mass spectrometry, *Nat Commun*, 12, 300, 10.1038/s41467-020-20532-2, 2021.
- Tröstl, J., Chuang, W. K., Gordon, H., Heinritzi, M., Yan, C., Molteni, U., Ahlm, L., Frege, C., Bianchi, F., Wagner, R., Simon, M., Lehtipalo, K., Williamson, C., Craven, J. S., Duplissy, J., Adamov, A., Almeida, J., Bernhammer, A. K., Breitenlechner, M., Brilke, S., Dias, A., Ehrhart, S., Flagan, R. C., Franchin, A., Fuchs, C., Guida, R., Gysel, M., Hansel, A., Hoyle, C. R., Jokinen, T., Junninen, H., Kangasluoma, J., Keskinen, H., Kim, J., Krapf, M., Kürten, A., Laaksonen, A., Lawler, M., Leiminger, M., Mathot, S., Möhler, O., Nieminen, T., Onnela, A., Petäjä, T., Piel, F. M., Miettinen, P., Rissanen, M. P., Rondo, L., Sarnela, N., Schobesberger, S., Sengupta, K., Sipilä, M., Smith, J. N., Steiner, G., Tomè, A., Virtanen, A., Wagner, A. C., Weingartner, E., Wimmer, D., Winkler, P. M., Ye, P., Carslaw, K. S., Curtius, J., Dommen, J., Kirkby, J., Kulmala, M., Riipinen, I., Worsnop, D. R., Donahue, N. M., and Baltensperger, U.: The role of low-volatility organic compounds in initial particle growth in the atmosphere, *Nature*, 533, 527-531, 10.1038/nature18271, 2016.
- Valiev, R. R., Hasan, G., Salo, V. T., Kubečka, J., and Kurten, T.: Intersystem Crossings Drive Atmospheric Gas-Phase Dimer Formation, *J Phys Chem A*, 123, 6596-6604, 10.1021/acs.jpca.9b02559, 2019.
- Vereecken, L. and Nozière, B.: H migration in peroxy radicals under atmospheric conditions, *Atmos Chem Phys*, 20, 7429-7458, 10.5194/acp-20-7429-2020, 2020.
- Vereecken, L. and Peeters, J.: Theoretical Study of the Formation of Acetone in the OH-Initiated Atmospheric Oxidation of α-Pinene, *J Phys Chem A*, 104, 11140-11146, 2000.
- Vereecken, L. and Peeters, J.: The 1,5-H-shift in 1-butoxy: A case study in the rigorous implementation of transition state theory for a multitoramer system, *J Chem Phys*, 119, 5159-5170, 10.1063/1.1597479, 2003.
- Vereecken, L. and Peeters, J.: Decomposition of substituted alkoxy radicals--part I: a generalized structure-activity relationship for reaction barrier heights, *Phys Chem Chem Phys*, 11, 9062-9074, 10.1039/b909712k, 2009.
- Vereecken, L. and Peeters, J.: A structure-activity relationship for the rate coefficient of H-migration in substituted alkoxy radicals, *Phys Chem Chem Phys*, 12, 12608-12620, 10.1039/c0cp00387e, 2010.
- Vereecken, L. and Peeters, J.: A theoretical study of the OH-initiated gas-phase oxidation mechanism of β-pinene (C₁₀H₁₆): first generation products, *Phys Chem Chem Phys*, 14, 3802-3815, 10.1039/c2cp23711c, 2012.
- Vereecken, L., Müller, J. F., and Peeters, J.: Low-volatility poly-oxygenates in the OH-initiated atmospheric oxidation of α-pinene: impact of non-traditional peroxy radical chemistry, *Phys Chem Chem Phys*, 9, 5241-5248, 10.1039/b708023a, 2007.

- Vereecken, L., Vu, G., Wahner, A., Kiendler-Scharr, A., and Nguyen, H. M. T.: A structure activity relationship for ring closure reactions in unsaturated alkylperoxy radicals, *Phys Chem Chem Phys*, 23, 16564-16576, 10.1039/d1cp02758a, 2021.
- Waring, M. S.: Secondary organic aerosol formation by limonene ozonolysis: Parameterizing multi-generational chemistry in ozone- and residence time-limited indoor environments, *Atmos Environ*, 144, 79-86, 10.1016/j.atmosenv.2016.08.051, 2016.
- 940 Wei, D., Fuentes, J. D., Gerken, T., Trowbridge, A. M., Stoy, P. C., and Chamecki, M.: Influences of nitrogen oxides and isoprene on ozone-temperature relationships in the Amazon rain forest, *Atmos. Environ.*, 206, 280-292, 10.1016/j.atmosenv.2019.02.044, 2019.
- Whalley, L. K., Edwards, P. M., Furneaux, K. L., Goddard, A., Ingham, T., Evans, M. J., Stone, D., Hopkins, J. R., Jones, C. E., Karunaharan, A., Lee, J. D., Lewis, A. C., Monks, P. S., Moller, S. J., and Heard, D. E.: Quantifying the magnitude of a missing hydroxyl radical source in a tropical rainforest, *Atmos. Chem. Phys.*, 11, 7223-7233, 10.5194/acp-11-7223-2011, 2011.
- 945 Williams, P. J. H., Boustead, G. A., Heard, D. E., Seakins, P. W., Rickard, A. R., and Chechik, V.: New Approach to the Detection of Short-Lived Radical Intermediates, *J Am Chem Soc*, 144, 15969-15976, 10.1021/jacs.2c03618, 2022.
- Xu, L., Møller, K. H., Crouse, J. D., Otkjær, R. V., Kjaergaard, H. G., and Wennberg, P. O.: Unimolecular Reactions of Peroxy Radicals Formed in the Oxidation of α -Pinene and β -Pinene by Hydroxyl Radicals, *J Phys Chem A*, 123, 1661-1674, 10.1021/acs.jpca.8b11726, 2019.
- 950 Xu, R., Thornton, J. A., Lee, B. H., Zhang, Y., Jaeglé, L., Lopez-Hilfiker, F. D., Rantala, P., and Petäjä, T.: Global simulations of monoterpene-derived peroxy radical fates and the distributions of highly oxygenated organic molecules (HOMs) and accretion products, *Atmos. Chem. Phys.*, 22, 5477-5494, 10.5194/acp-22-5477-2022, 2022.
- 955 Yan, C., Nie, W., Äijälä, M., Rissanen, M. P., Canagaratna, M. R., Massoli, P., Junninen, H., Jokinen, T., Sarnela, N., Häme, S. A. K., Schobesberger, S., Canonaco, F., Yao, L., Prévôt, A. S. H., Petäjä, T., Kulmala, M., Sipilä, M., Worsnop, D. R., and Ehn, M.: Source characterization of highly oxidized multifunctional compounds in a boreal forest environment using positive matrix factorization, *Atmos Chem Phys*, 16, 12715-12731, 10.5194/acp-16-12715-2016, 2016.
- Yan, C., Nie, W., Vogel, A. L., Dada, L., Lehtipalo, K., Stolzenburg, D., Wagner, R., Rissanen, M. P., Xiao, M., Ahonen, L., Fischer, L., Rose, C., Bianchi, F., Gordon, H., Simon, M., Heinritzi, M., Garmash, O., Roldin, P., Dias, A., Ye, P., Hofbauer, V., Amorim, A., Bauer, P. S., Bergen, A., Bernhammer, A. K., Breitenlechner, M., Brilke, S., Buchholz, A., Mazon, S. B., Canagaratna, M. R., Chen, X., Ding, A., Dommen, J., Draper, D. C., Duplissy, J., Frege, C., Heyn, C., Guida, R., Hakala, J., Heikkinen, L., Hoyle, C. R., Jokinen, T., Kangasluoma, J., Kirkby, J., Kontkanen, J., Kurten, A., Lawler, M. J., Mai, H., Mathot, S., Mauldin, R. L., Molteni, U., Nichman, L., Nieminen, T., Nowak, J., Ojdanic, A., Onnela, A., Pajunoja, A., Petaja, T., Piel, F., Quelever, L. L. J., Sarnela, N., Schallhart, S., Sengupta, K., Sipilä, M., Tome, A., Trostl, J., Vaisanen, O., Wagner, A. C., Ylisirnio, A., Zha, Q., Baltensperger, U., Carslaw, K. S., Curtius, J., Flagan, R. C., Hansel, A., Riipinen, I., Smith, J. N., Virtanen, A., Winkler, P. M., Donahue, N. M., Kerminen, V. M., Kulmala, M., Ehn, M., and Worsnop, D. R.: Size-dependent influence of NO_x on the growth rates of organic aerosol particles, *Sci Adv*, 6, ARTN eaay4945 10.1126/sciadv.aay4945, 2020.
- 960 T., Piel, F., Quelever, L. L. J., Sarnela, N., Schallhart, S., Sengupta, K., Sipilä, M., Tome, A., Trostl, J., Vaisanen, O., Wagner, A. C., Ylisirnio, A., Zha, Q., Baltensperger, U., Carslaw, K. S., Curtius, J., Flagan, R. C., Hansel, A., Riipinen, I., Smith, J. N., Virtanen, A., Winkler, P. M., Donahue, N. M., Kerminen, V. M., Kulmala, M., Ehn, M., and Worsnop, D. R.: Size-dependent influence of NO_x on the growth rates of organic aerosol particles, *Sci Adv*, 6, ARTN eaay4945 10.1126/sciadv.aay4945, 2020.
- 965 T., Piel, F., Quelever, L. L. J., Sarnela, N., Schallhart, S., Sengupta, K., Sipilä, M., Tome, A., Trostl, J., Vaisanen, O., Wagner, A. C., Ylisirnio, A., Zha, Q., Baltensperger, U., Carslaw, K. S., Curtius, J., Flagan, R. C., Hansel, A., Riipinen, I., Smith, J. N., Virtanen, A., Winkler, P. M., Donahue, N. M., Kerminen, V. M., Kulmala, M., Ehn, M., and Worsnop, D. R.: Size-dependent influence of NO_x on the growth rates of organic aerosol particles, *Sci Adv*, 6, ARTN eaay4945 10.1126/sciadv.aay4945, 2020.
- 970 Yu, J., Cocker III, D. R., Griffin, R. J., Flagan, R. C., and Seinfeld, J. H.: Gas-phase ozone oxidation of monoterpenes: Gaseous and particulate products, *J Atmos Chem*, 34, 207-258, Doi 10.1023/A:1006254930583, 1999.
- Zhang, H., Yee, L. D., Lee, B. H., Curtis, M. P., Worton, D. R., Isaacman-VanWertz, G., Offenberg, J. H., Lewandowski, M., Kleindienst, T. E., Beaver, M. R., Holder, A. L., Lonneman, W. A., Docherty, K. S., Jaoui, M., Pye, H. O. T., Hu, W., Day, D. A., Campuzano-Jost, P., Jimenez, J. L., Guo, H., Weber, R. J., de Gouw, J., Koss, A. R., Edgerton, E. S., Brune, W., 975 Mohr, C., Lopez-Hilfiker, F. D., Lutz, A., Kreisberg, N. M., Spielman, S. R., Hering, S. V., Wilson, K. R., Thornton, J. A., and Goldstein, A. H.: Monoterpenes are the largest source of summertime organic aerosol in the southeastern United States, *Proc Natl Acad Sci U S A*, 115, 2038-2043, 10.1073/pnas.1717513115, 2018.

- 980 Zhao, B., Shrivastava, M., Donahue, N. M., Gordon, H., Schervish, M., Shilling, J. E., Zaveri, R. A., Wang, J., Andreae, M. O., Zhao, C., Gaudet, B., Liu, Y., Fan, J., and Fast, J. D.: High concentration of ultrafine particles in the Amazon free troposphere produced by organic new particle formation, *Proc. Nat. Acad. Sci. U.S.A.*, 117, 25344-25351, 10.1073/pnas.2006716117 %J Proceedings of the National Academy of Sciences, 2020.
- Zhao, D., Pullinen, I., Fuchs, H., Schrade, S., Wu, R., Acir, I.-H., Tillmann, R., Rohrer, F., Wildt, J., Guo, Y., Kiendler-Scharr, A., Wahner, A., Kang, S., Vereecken, L., and Mentel, T. F.: Highly oxygenated organic molecule (HOM) formation in the isoprene oxidation by NO₃ radical, *Atmos Chem Phys*, 21, 9681-9704, 10.5194/acp-21-9681-2021, 2021.
- 985 Zhao, D., Schmitt, S. H., Wang, M., Acir, I.-H., Tillmann, R., Tan, Z., Novelli, A., Fuchs, H., Pullinen, I., Wegener, R., Rohrer, F., Wildt, J., Kiendler-Scharr, A., Wahner, A., and Mentel, T. F.: Effects of NO_x and SO₂ on the secondary organic aerosol formation from photooxidation of α -pinene and limonene, *Atmos Chem Phys*, 18, 1611-1628, 10.5194/acp-18-1611-2018, 2018a.
- Zhao, D. F., Buchholz, A., Kortner, B., Schlag, P., Rubach, F., Kiendler-Scharr, A., Tillmann, R., Wahner, A., Flores, J. M., 990 Rudich, Y., Watne, Å. K., Hallquist, M., Wildt, J., and Mentel, T. F.: Size-dependent hygroscopicity parameter (κ) and chemical composition of secondary organic cloud condensation nuclei, *Geophys Res Lett*, 42, 10,920-910,928, 10.1002/2015gl066497, 2015a.
- Zhao, D. F., Kaminski, M., Schlag, P., Fuchs, H., Acir, I. H., Bohn, B., Häseler, R., Kiendler-Scharr, A., Rohrer, F., Tillmann, R., Wang, M. J., Wegener, R., Wildt, J., Wahner, A., and Mentel, T. F.: Secondary organic aerosol formation from hydroxyl 995 radical oxidation and ozonolysis of monoterpenes, *Atmos Chem Phys*, 15, 991-1012, 10.5194/acp-15-991-2015, 2015b.
- Zhao, Y. and Truhlar, D. G.: The M06 suite of density functionals for main group thermochemistry, thermochemical kinetics, noncovalent interactions, excited states, and transition elements: two new functionals and systematic testing of four M06-class functionals and 12 other functionals, *Theor Chem Account*, 120, 215-241, 10.1007/s00214-007-0310-x, 2008.
- Zhao, Y., Thornton, J. A., and Pye, H. O. T.: Quantitative constraints on autoxidation and dimer formation from direct probing 1000 of monoterpene-derived peroxy radical chemistry, *Proc Natl Acad Sci U S A*, 115, 12142-12147, 10.1073/pnas.1812147115, 2018b.
- Ziemann, P. J. and Atkinson, R.: Kinetics, products, and mechanisms of secondary organic aerosol formation, *Chem Soc Rev*, 41, 6582-6605, 10.1039/c2cs35122f, 2012.